CD20 as target for immunotherapy

Engelberts, P.J.

6

DuoBody®-CD3xCD20, an Fc-silenced whole IgG T cell retargeting bispecific antibody, displays unique capacity to induce T-cell mediated kill of malignant B cells, and provides opportunities for subcutaneous dosing

- Patrick J. Engelberts[1,2], Ida H. Hiemstra[1], Joyce Meesters[1], Bart de Jong[1], Irati Beltran Hernandez[1], Simone Oostindie[1,2], Bart-Jan de Kreuk[1], Edward N. van den Brink[1] , Theodora Salcedo[1], Sandra Verploegen[1], Aran F. Labrijn[1], Sjeng Horbach[1], Janine Schuurman[1], Esther C.W. Breij[1]* and Paul W.H.I Parren[1,2,3]

1 Genmab, Utrecht, The Netherlands

2 Department of Hematology and Blood Transfusion, Leiden University Medical Center, Leiden, the Netherlands

3 current affiliation: Lava Therapeutics, 's Hertogenbosch, The Netherlands

* Corresponding author: Esther Breij

ABSTRACT

With the aim to develop a CD3 bispecific antibody (bsAb) for the treatment of B-cell malignancies, we employed an *in vitro* functional screen to test a panel of CD3 bsAbs that were generated by controlled Fab-arm exchange and were derived from antibodies against a set of B-cell surface antigens with medium-to-high expression on B-cell lymphomas.

Neither antigen expression density nor antibody affinity appeared to correlate with *in vitro* potency of the tested bsAb. One combination of a human CD20 antibody paired with our CD3 bsAb platform was identified as an extraordinary potent B cell-targeting CD3 bsAb. This CD3xCD20 bsAb was able to activate both $CD4^+$ and $CD8^+$ T cells, as determined by increased CD25 and CD69 expression, and to induce *in vitro* cytotoxicity at low antibody concentrations. The activation of T cells was conditional and only occurred when $CD20^+$ cells, $CD3^+$ cells and the CD3xCD20 bsAb were present.

In vivo studies in mice showed that this CD3 bsAb efficiently depleted $CD20^+$ cells both from circulation as well as from solid tumor mass.

Safety and efficacy studies in cynomolgus monkeys revealed long-lasting but reversible B cell depletion from blood and secondary lymphoid structures, with-time-to-recovery inversely related to the treatment dose. Furthermore, relative to IV administration, SC administration of the CD3 bsAb was associated with reduction in plasma cytokine levels and lower C_{max} levels, while maintaining long lasting B cell depletion from circulation and lymphoid structures similar in magnitude.

This CD3xCD20 bsAb (DuoBody-CD3xCD20, GEN3013) was selected for clinical development and a first-in-human study has been initiated.

INTRODUCTION

Bispecific antibodies (bsAbs) specifically recognizing CD3 in addition to a tumor-associated antigen (TAA), the CD3 bsAbs, have begun to deliver their promise in the development of cancer treatments. The bispecific T-cell engager (BiTe) blinatumomab, a CD3xCD19 single-chain bsAb molecule, recently obtained regulatory approval from the US Food and Drug Administration (FDA) for use in relapsed or refractory acute lymphoblastic leukemia (ALL) following its initial accelerated approval in 2014 [1]. The complete response (CR) rates of 43% in ALL and 19% in diffuse large B-cell lymphoma (DLBCL) observed after treatment with blinatumomab clearly demonstrate the potential of CD3 bsAbs in these malignancies [2].

Room for advancing the CD3 bsAb approach exists both in terms of improving the bsAb format to optimize plasma half-life and manufacturability, as well as in terms of further expanding the arsenal of TAA that can be used as targets for CD3 bsAbs in the clinic. Indeed, CD3 bsAbs targeting a variety of TAA in numerous formats are currently being investigated, yet it remains hard to predict the optimal combination of TAA and bsAb format that generates the most effective CD3 bsAb.

Many factors contribute to the potency, safety and corresponding therapeutic window of CD3 bsAbs. In preclinical models, an important factor contributing to potency is the cell membrane proximity of the epitope

recognized by the tumor-targeting arm of the CD3 bsAb. A number of studies have shown that tumor cell killing capacity increases when binding of CD3 bsAbs to their specific TAA occurs closer to the target cell membrane [3, 4]. Moreover, the format of the CD3 bsAb may impact the potency of the therapeutic. For example, differences in cytotoxic activity were observed when the same pair of CD3xCD19 antigen-binding domains was used in either the BiTe or the dual-affinity re-targeting (DART) bsAb platforms, both of which are based on scFv Ab fragments connected by linkers. The less flexible DART CD3xCD19 bsAb demonstrated superior activity over the corresponding BiTe bsAb molecule [5]. TAA characteristics, such as abundance [6, 7], size, molecular flexibility [3] and mobility, macromolecular organization and accessibility may all contribute to CD3 bsAb potency making it nearly impossible to rationalize target and epitope choice at this point in time.

We previously developed a method to generate bsAbs using controlled Fab-arm exchange (cFAE), termed DuoBody technology. Here, two parental IgG1 antibodies, each with a matched single point mutation in the IgG Fc domain, controllably reorganize into bispecific IgG1 molecules upon exposure to tailored manufacturing conditions [8, 9]. The cFAE process has been shown to be an easy and robust method to generate highly stable bsAbs with superior yield compared to other bsAb platforms, both at research and manufacturing scale [10]. Importantly, the method provides the opportunity to rapidly generate large panels of bispecific antibodies targeting different antigens and/or epitopes, allowing functional screening to identify antibody pairs with optimal characteristics when combined in a bsAb. We set out to generate a CD3 bsAb specifically targeting CD20, a well-known and clinically validated target for the treatment of B cell malignancies. DuoBody-CD3xCD20 (GEN3013) is a bispecific antibody recognizing the T-cell antigen CD3 and the B-cell antigen CD20, that was generated with cFAE of a humanized version of anti-CD3 antibody SP34 (huCACAO) [11] and human anti-CD20 antibody 7D8 [12]. Various (combinations of) mutations to abrogate interactions of the IgG Fc domain with FcγR and complement were evaluated to prevent T cell activation through antibody-mediated FcγR-dependent crosslinking of CD3 in the absence of target cells. DuoBody-CD3xCD20 induced potent T cell activation and T cell cytotoxic activity in the presence of cell lines from B cell malignancies in vitro. With the aim to explain its excellent potency *in vitro* in the context of the CD20-specific Fab-arm, CD3 bsAb generated using IgG1-7D8 were compared to alternative CD3 bsAb targeting CD20 or other B cell antigens an *in vitro* screen. Anti-tumor activity of DuoBody-CD3xCD20 was confirmed *in vivo* in humanized mouse models. The pharmacokinetic (PK) properties and its capacity to induce B cell depletion, after either intravenous or subcutaneous administration, were assessed in cynomolgus monkeys as part of the non-clinical safety studies.

MATERIAL & METHODS

Cell lines

Human B-cell lymphoma cell lines were obtained from the Deutsche Sammlung von Mikroorganismen und Zellkulturen (DSMZ): OCI-Ly7, SU-DHL-4, RI-1, JEKO-1, WSU-DLCL2, U-2932, OCI-Ly18, RC-K8, OCI-Ly19 and SU-DHL-8 or from the American Tissue Culture Collection (ATCC): Raji, Daudi and Z138. Daudi and Raji cells were transfected with gWIZ luciferase as previously described [13]. Cell lines were cultured according to suppliers' instructions.

Antibodies

CD3- and TAA-specific Abs were recombinantly produced in a human IgG1 backbone as described [14], with the insertion of an F405L mutation in all CD3 monoclonal Abs (mAbs) and a K409R mutation in all tumor targeting Abs [15] (Table 1). The F405L and K409R mutations do not affect functional Ab characteristics under normal physiological conditions [8]. BsAbs targeting CD3 and a B cell target were generated by cFAE as described previously [9]. Control bsAbs binding only CD3 (bsAb-CD3xctrl) or only CD20 (bsAb-ctrlxCD20) were generated by cFAE of CD3 or CD20 mAbs, respectively, with the HIV-1 gp120 specific antibody IgG1-b12 [16].
Commercially available antibodies used for flow cytometry and confocal microscopy analyses are listed in supplemental Table 1.

Isolation of PBMC and T cells from healthy donors

Buffycoats from healthy donors obtained from Sanquin (Amsterdam) were used to isolate either PBMCs using Lymphocyte separation medium (Lonza, Bazel, Switzerland) or pan-T-cells, $CD4^+$ T cells or $CD8^+$ T cells by negative selection using RosetteSEP™ Enrichment cocktail kits (Stem Cell Technologies, Vancouver, Canada). Purity of all fractions after isolation was measured by flow cytometry.

Chromium release assay to assess T cell-mediated cytotoxicity

Chromium release assay was performed as previously described in da Roit *et al.* [17]. Specific lysis was calculated as: % specific lysis = ((CPM sample – CPM background lysis) / (CPM maximal lysis – CPM background lysis)) x 100, where CPM refers to counts per minute. ^{51}Cr release was measured using a gamma counter (Cobra model C5002; PackardPerkinElmer).

Flow cytometry analysis to assess T cell activation and T cell-mediated cytotoxicity

Isolated T cells were incubated with Ab and tumor cell lines (E:T ratio 2:1) in assay medium (RPMI 1640, supplemented with 1% Penicillin/Streptomycin (both from LONZA) and 10% Cosmic Calf Serum (Perbio)) for 48 h. Alternatively, PBMCs (containing both effector and target cells) were incubated in assay medium with for 72 h. After the incubation period, cells were washed in FACS buffer (PBS with 0.1% bovine serum albumin (BSA, Roche) and 0.02% NaN_3 (Sigma Aldrich)), stained with Abs for T cell (activation and phenotype) and B cell marker (CD19) (listed in supplemental Table 1) at 4°C for 30 min, washed again, after which a fixed sample volume (80 mL) was measured on a BD LSRFortessa™ cell analyzer (BD Biosciences, San Jose, CA, USA). Data were

TABLE 1 Antibody clones used in this study and their respective origin.

Target	Clone	Described by
CD3	CLB	Parren et al. [30]
	huCACAO	Genmab
CD20	2C6	Genmab
	7D8	Genmab
	RTX	Roche
	hu2H7	Genentech
CD22	RFB4	US Government of Health and Human Services/Ira Pastan
CD24	SWA11	Medical Research Infrastructure/Arber Nadir
CD70	1F6	Seattle Genetics
	1F4	Medarex
	2H5	Medarex
	10B4	Medarex
CD37	37-3	Immunogen
	G28-1	Boehringer Ingelheim
	Ab1	undisclosed
	Ab2	undisclosed
	Ab3	undisclosed
	Ab4	undisclosed
CD79b	SN8v28	Genentech
CD138	nBT062	Biotest/Immunogen
HLA-DR	1-D09C03	Massachusetts Institute of Technology/ Gpc Biotech/Morphosys
	K8-355	Abbvie/Abbott/Facet/Pdl/Protein Design Labs
	1D10	
	4	Abbvie/Abbott/Facet/Pdl/Protein Design Labs
	L243 / huL243	Immunomedics
HER2	169	Genmab

analyzed using FlowJo® software V10.1 (Ashland, OR, USA). The percentage of activated $CD4^+$ or $CD8^+$ T cells was determined by gating those cells that expressed activation markers CD69 or CD25 as well. For cytotoxicity experiments with isolated T cells, the number of intact, surviving B cells was gated as $CD4^-$ and $CD8^-$ negative cells, with an unaltered FSC/SSC phenotype. For cytotoxicity experiments with PBMCs, the B cells were in addition gated for CD19 positivity. % cell kill was calculated as follows: 100 – (($\text{cell count}_{\text{sample}}$/$\text{cell count}_{\text{medium}}$) x 100%).

Fluorescence confocal microscopy

Daudi cells were labeled with CellTracker Deep Red (Invitrogen, Carlsbad, California, USA), according to the manufacturer's instruction and incubated on a Cell-Tak

(Corning) coated chamber slide (Thermo Scientific Nunc) for 30 min at 37°C, followed by incubation with T cells (1:1 ratio, 24 h). As a control, the Daudi - T cell coculture was performed in the absence of Ab. Samples were fixed in 2% formaldehyde at RT for 10 min. For detection of CD69 or bound DuoBody-CD3xCD20, staining was performed at RT for 45 min. For intracellular staining of perforin or granzyme B, cells were permeabilized with Cytofix/Cytoperm solution (BD Biosciences) at 4°C for 20 min. All samples were washed with PBS and mounted using vectashield (with DAPI, Vector Laboratories). Images were taken with a confocal laser scanning microscope Nikon A1R/STORM and a 60x objective (Apo 60x Oil λS DIC N2). Acquired images were processed with ImageJ [18].

In vivo mouse models

A PBMC co-engraftment xenograft model was performed analogous to the model described by Brischwein *et al*. [19]. In brief, at day 0 female non-obese diabetic/severe combined immunodeficiency (NOD-SCID) mice were inoculated with a mixture of 5 x 10^6 PBMCs and 5 x 10^6 Raji-luc Burkitt's lymphoma tumor cells in a total volume of 200 µL, subcutaneously (SC) on the right flank. Immediately after the injection, mice were treated intravenous (IV) with Ab as described. At least twice per week, mice were checked for clinical signs of illness and tumor volume was determined from caliper measurements (tumor volume [mm^3] = 0.52 x [length] x [width]^2).

The humanized immune system (HIS) model was generated by inoculating 10^6 $CD34^+$ hematopoietic stems cells intrahepatically in BALB/c $Rag2^{tm1Fwa}$ IL-$2Rg_c^{tm1Cgn}$ $SIRP\alpha^{NOD}$ (BRGS) mice as described [20]. After 14-15 weeks, BRGS-HIS mice were inoculated with 5 x10^6 Burkitt's lymphoma tumor Daudi-luc cells IV or Raji-luc cells SC (indicated as day 0 of the study). Mice were randomized (n=7 per group) and IV injected biweekly (Q2Wx2 or Q2Wx5 respectively) with Ab or PBS as described, starting at day 3. Tumor growth was evaluated weekly by bioluminescence imaging (BLI) or by caliper measurements. In addition, the number of B cells and the activation status of T cells in blood were analyzed by flow cytometry on day 9, as described above.
All animal experiments were performed in compliance with European directives (2010/63/EU) and are approved by the local Ethical committees.

Toxicology studies in cynomolgus monkeys

Non-clinical safety and pharmacology studies were conducted at Charles River Laboratories (Tranent, UK) in accordance with the European Convention for the Protection of Vertebrate Animals Used for Experimental and Other Scientific Purposes (Council of Europe), under control of the UK Home Office. Cynomolgus monkeys received DuoBody-CD3xCD20 either via IV infusion or SC injection.
Whole blood samples (approximately 0.5 mL) were collected from the femoral vein. Plasma was isolated by centrifugation of whole blood samples at 3000 rpm (approximately 1500 g) for 10 minutes at 4°C. Biopsies (approximately 20 mg) were taken from superficial lymph nodes by cutting down onto the lymph node using standard surgical aseptic techniques, while the ani-

mals were under general anesthesia. Single cell suspensions were prepared using the Medimachine System for automated, mechanical disaggregation of tissues (Becton Dickinson).

DuoBody-CD3xCD20 plasma concentrations were determined with a single molecule counting (SMC) method, a fluorescent sandwich immunoassay technique, that is validated and performed at PRA Health Sciences Bioanalytical Laboratory (PRA), Assen, The Netherlands.

The concentrations of IL-1β, IL-2, IL-6, IL-4, IL-8, IL-10, IL-12p40, IL-15, IFNγ, TNFα and MCP-1 in plasma were analyzed using the Milliplex MAP NHP Cytokine Magnetic Bead Panel (Millipore Cat. No. PRCYTOMAG-40K) for use with a BioPlex 200 reader (BioRad) according to the manufacturers' protocol.

The number of B cells present in whole blood samples or single cell suspensions obtained from lymph node biopsies was determined by flow cytometry analysis using a two-laser five-color Beckman Coulter FC500 or a BD LSR Fortessa X, gating for $CD19^+$ cells (antibodies used are indicated in supplementary table 1).

Data analysis and statistics

Dose-response curves were generated using four-parameter non-linear regression analysis (GraphPad Prism 7.02 software [La Jolla, CA, USA]; equation log[agonist] vs. response – variable slope). Ab concentrations that induce 50 percent of the maximal response (EC_{50} values) were derived from these curves.

For statistics on mouse *in vivo* data, differences were analyzed by Mann-Whitney two-tailed test versus PBS or Kruskall-Wallis analysis of variance test (ANOVA) with Dunn's multiple comparisons test as indicated.

RESULTS

Silencing of IgG Fc domain and functional characterization of bsAb CD3xCD207D8 *in vitro*

The presence of an Fc region in CD3 bsAbs is considered attractive for therapeutic antibody development due to the favorable pharmacokinetic characteristics and relatively straightforward manufacturability process [10]. However, a fully functional IgG1 Fc domain is less attractive for CD3 bsAbs, because antibody-dependent FcγR-mediated CD3 cross-linking might induce TAA-independent T cell activation. To avoid TAA-independent T cell activation in PMBCs, we set out to identify mutations in the IgG Fc domain that could silence Fc-mediated effector functions, while retaining FcRn binding and being compatible with controlled Fab-arm exchange (Supplemental Figure 1). It was shown that introduction of a combination of three mutations, L234F, L235E and D265A (FEA) into the IgG constant domain, resulted in the best silencing and PK. These mutations did not affect binding to the target (supplemental Figure 1A). CD3 mAbs carrying the FEA mutations were unable to induce antibody-mediated FcγR-dependent T cell activation and proliferation in PBMCs (Supplemental Figure 1B and 1C). Moreover, by introduction of these mutations in IgG1-CD3, bsAb-CD3xctrl or bsAb-CD3xTAA, TAA-independent lysis of tumor cells could be prevented (Supplemental Figure 1D, E and F, respectively). Furthermore, Fc silencing also prevented TAA-independent release

of cytokines (Supplemental Figure 1G). CD3 mAbs (and CD3 bsAbs) carrying the FEA mutations were unable to bind FcγR and C1q (supplemental Figure 1H and I). Fc silencing mutations did not affect *in vivo* half-life (Supplemental Figure 1J, K).

Functional characterization of DuoBody-CD3xCD20 *in vitro*

To generate a CD3xCD20 bsAb molecule that induces T cell-mediated cytotoxicity exclusively in the presence of CD20-positive cells, the FEA mutations were introduced into a humanized variant of the CD3-specific antibody SP34 and the human CD20-specific antibody IgG1-7D8 and bispecific molecules were generated using cFAE. The resulting CD3 bsAb, designated DuoBody-CD3xCD20 (GEN3013), was functionally characterized *in vitro*.

Upon incubation with PBMCs, DuoBody-CD3xCD20 induced T cell activation, as indicated by a dose-dependent increase in CD69 expression on both $CD4^+$ and $CD8^+$ T cells (Figure 1A, left and middle panel), that coincided with kill of endogenous $CD20^+$ B cells from PBMC (Figure 1A, right panel). Neither monovalent control bsAb (bsAb-CD3xctrl or bsAb-ctrlxCD20, carrying either the CD3- or the CD20-specific Fab-arm, respectively) was able to induce T cell activation or B cell depletion in PBMCs. This demonstrates that DuoBody-CD3x-CD20-mediated T cell activation and cytotoxic activity are strictly dependent on binding to both CD3 and CD20. Consistent with this observation, T cell-B cell doublets were observed in PBMCs in the presence of DuoBody-CD3xCD20, but not in the presence of monovalent or monospecific control Abs (Supplemental Figure 2A). The capacity of DuoBody-CD3xCD20 to induce T cell-mediated cytotoxicity in malignant B cells was assessed in a panel of B cell lymphoma cell lines, with CD20 cell surface expression ranging from 33,000 to 350,000 sABC (Table 2). DuoBody-CD3xCD20 induced potent cytotoxicity in all tumor cell lines tested (Table 2 for all cell lines; Figure 1B for Daudi cells). DuoBody-CD3xCD20, but not the control Ab bsAb-CD3xctrl, induced highly potent and dose-dependent cytotoxicity using total T cells (EC_{50} 0.63 ng/mL), $CD4^+$ T cells (EC_{50} 0.64 ng/mL) or $CD8^+$ T cells (EC_{50} 0.13 ng/mL) as effector cells and Daudi cells as target cells (Figure 1C), as measured in a chrome release assay. There was no correlation between CD20 expression levels and efficacy of DuoBody-CD3x-CD20-mediated cytotoxicity in this cell line panel (Table 2).

DuoBody-CD3xCD20 induced activation and cytotoxic activity of both $CD4^+$ and $CD8^+$ T cells, but the dynamics were different between the two populations (Figure 1C). While activation of $CD4^+$ and $CD8^+$ T cells, as assessed by CD69 (Figure 1D) and CD25 expression (supplemental figure 2B), occurred in a similar timeframe, cytotoxicity mediated by $CD4^+$ T cells was delayed compared to that mediated by $CD8^+$ T cells (Figure 1C). For $CD4^+$ T cells, cytotoxicity was first observed after 24 hours of incubation and increased up to 48 hours. $CD8^+$ T cell-mediated cytotoxicity could already be measured after three hours and increased up to 24 hours, with no further increase at 48 hours. The observed EC_{50} for T cell activation was in agreement with the observed earlier onset and more potent cytotoxicity induction of $CD8^+$ T cells compared to $CD4^+$ T cells, as EC_{50} for cytotoxicity induced by

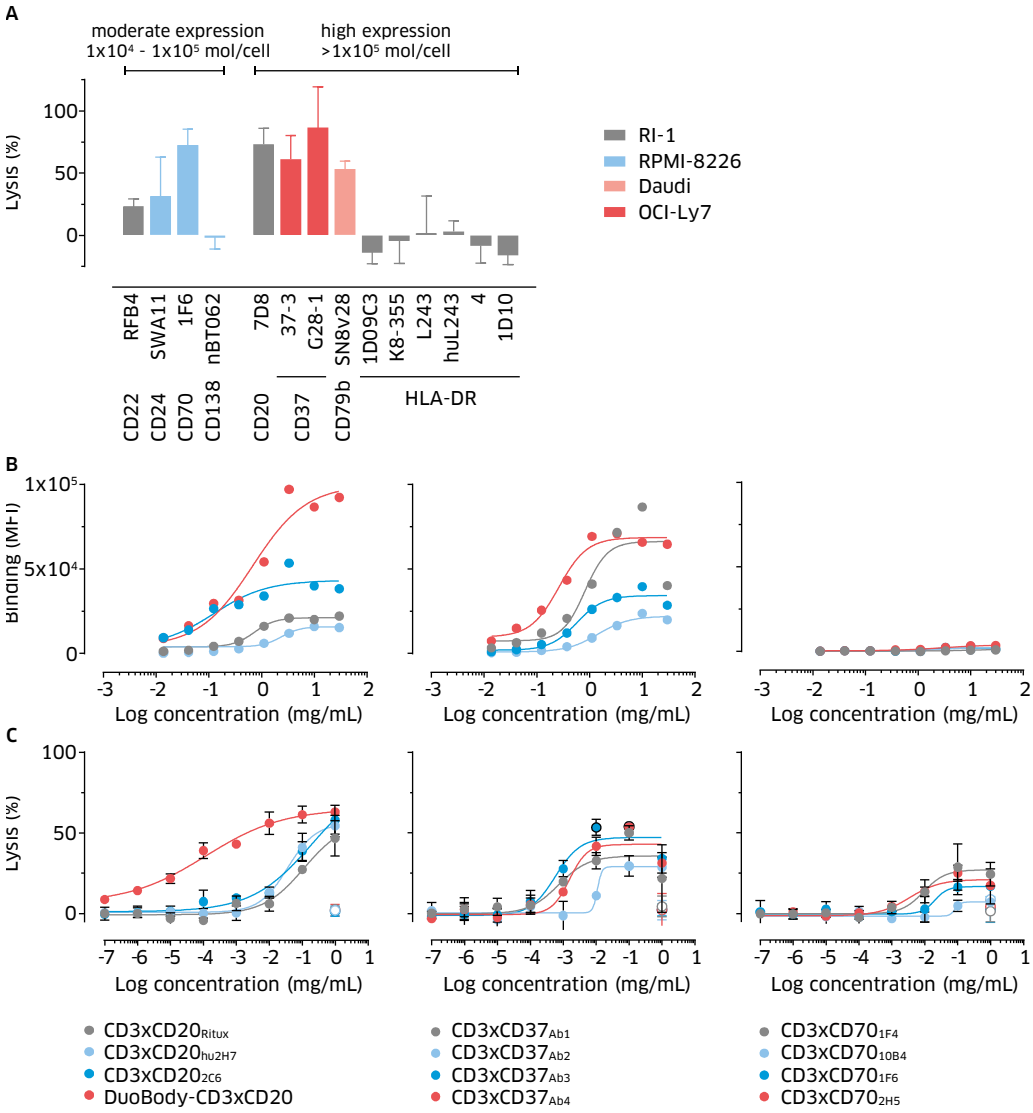

D

B-cell target	bsAbs	Binding EC_{50} (mg/mL ± SD)	Cytotoxocity EC_{50} (mg/mL ± SD)
CD20	$CD3xCD20_{Ritux}$	1.046 ± 0.582	0.071 ± 0.046
	$CD3xCD20_{hu2H7}$	1.265 ± 0.378	0.035 ± 0.021
	$CD3xCD20_{2C6}$	0.186 ± 0.102	0.083 ± 0.105
	DuoBody-CD3xCD20	0.661 ± 0.518	0.014 ± 0.024
CD37	$CD3xCD37_{Ab3}$	0.622 ± 0.267	0.010 ± 0.016
	$CD3xCD37_{Ab4}$	0.524 ± 0.120	0.086 ± 0.096
	$CD3xCD37_{Ab2}$	0.783 ± 0.307	0.125 ± 0.209
	$CD3xCD37_{Ab1}$	0.233 ± 0.039	0.016 ± 0.021
CD70	$CD3xCD70_{1F4}$	ND	0.142 ± 0.176
	$CD3xCD70_{10B4}$	ND	ND
	$CD3xCD70_{1F6}$	ND	0.141 ± 0.220
	$CD3xCD70_{2H5}$	ND	0.035 ± 0.038

FIGURE 1 **Functional characterization of DuoBody-CD3xCD20 *in vitro*.**
A: PBMCs were incubated with antibody for 72 h. The percentages of CD69-positive $CD4^+$ (**left**) and $CD8^+$ T cells (**middle**) and the remaining number of intact endogenous B cells (**right**) were determined by flow cytometry with the gating strategy and formula explained in M&M. Data shown are from one representative experiment out of 4 performed and are mean percentages ± SEM of duplicate wells.
B: Isolated $CD4^+$ T cells, $CD8^+$ T cells or total T cells were incubated with DuoBody-CD3xCD20 (**left**) or bsAb-CD3xctrl (**right**) and chromium labeled Daudi cells for 48h. Between brackets the effector: target (E:T) ratio is indicated. Alternatively $CD4^+$ T cells (**C**, **left**) or $CD8^+$ T cells (**C**, **right**) were incubated with DuoBody-CD3xCD20 and chromium labeled Daudi cells for the indicated periods of time (E:T, 20:1). Data shown are mean percentages lysis ± SEM of triplicates. Data from one representative experiment is shown.
D: Freshly isolated T cells were incubated with DuoBody-CD3xCD20 and CD20-expressing Daudi cells (E:T ratio 2:1). Percentages of CD69-positive $CD4^+$ (**left**) and $CD8^+$ T cells (**right**) were determined at different time points, using the gating strategy indicated in M&M. Data for one representative donor out of four donors are shown. Graphs show the mean ± SEM of duplicate wells.
E: Isolated T cells were co-cultured with Daudi cells in the presence of DuoBody-CD3xCD20 for 24 h after which images were taken. Images shown are a 60x magnification (with an extra optical magnification in **the most left picture of the panel**) and representative of at least 3 experiments.

TABLE 2 **Average EC50 values of DuoBody-CD3xCD20-induced T-cell-mediated cytotoxicity towards B-cell lymphoma cell lines with different levels of CD20 expression.**

Cell line		CD20 expression level (number of molecules/cell)			Average EC_{50} [SD] of cytotoxicity (% kill – flow cytometry assay)		
Name	Lymphoma type	Average (*1000)	Range (*1000)	n tests	ng/mL	pM	n donors
OCI-Ly7	GCB	350	209-453	6	0.531 [0.813]	3.540 [5.420]	3
Daudi	BL	331	97-752	11	0.039 [0.022]	0.260 [0.147]	11
SU-DHL-4	GCB	308	101-715	7	0.031 [0.000]	0.207 [0.000]	2
RI-1	ABC	240	150-356	4	0.066 [0.083]	0.440 [0.553]	6
JEKO-1	MCL	233	159-276	3	0.089 [0.033]	0.593 [0.220]	4
WSU-DL-CL2	GCB	233	144-330	4	0.116 [0.030]	0.773 [0.200]	4
U-2932	ABC	180	85-241	4	67.604 [114.929]	450.693 [766.193]	4
OCI-Ly18	GCB	166	84-237	4	0.057 [0.042]	0.380 [0.280]	3
RC-K	ABC	139	78-223	4	0.743 [0.673]	4.953 [4.487]	2
Z-138	MCL	90	53-114	5	0.057 [0.023]	0.380 [0.153]	2
OCI-Ly19	GCB	36	0-62	4	0.181 [0.086]	1.207 [0.573]	2
SU-DHL-8	GCB	33	0-88	8	0.120 [0.105]	0.800 [0.700]	2

Averages of CD20 expression levels and EC_{50} values of DuoBodyCD3xCD20-induced Tcellmediated cytotoxicity measurements for each B-cell lymphoma cell line tested, calculated from multiple experiments.

(GCB = germinal center B-cell diffuse large B-cell lymphoma, ABC = activated B-cell diffuse large B-cell lymphoma, BL = Burkitt's lymphoma, MCL = mantle-cell lymphoma, n = the number of donors with complete dose-response curves).

CD8+ T cells was lower as than for CD4+ T cells. BsAb-CD3xctrl was unable to activate T cells, as assessed by CD69 and CD25 expression (supplemental figure 2C). Confocal microscopy analysis of T cell-Daudi cell co-cultures that had been incubated with DuoBody-CD3xCD20 confirmed expression of CD69 on CD4+ and CD8+ T cells that were in close proximity of Daudi cells (Figure 2E). Moreover, perforin accumulation was observed in both CD4+ and CD8+ T cells that were associated with CD20-positive tumor cells, indicating cytotoxic granule upregulation.

In summary, DuoBody-CD3xCD20 induced efficient kill of CD20-positive cells, which was mediated by both CD4+ and CD8+ T cells. T cell activation and cytotoxic activity were strictly dependent on binding to both CD3 and CD20.

Studying the contribution of the CD20-specific Fab-arm to the potency of DuoBody-CD3xCD20

With the aim to explain the excellent potency of DuoBody-CD3xCD20 in the context of the CD20-specific Fab-arm derived from the CD20 antibody 7D8 [12, 21], we compared the binding and cytotoxic potential of a CD3 bsAb with a 7D8-derived Fab-arm with a panel of CD3 bsAbs generated using alternative CD20-specific Fab arms or Fab-arms directed against a multitude of B cell antigens.

The cell-surface expression of different B cell antigens on cell lines representing a range of human B cell malignancies was assessed by quantitative flow cytometry (Supplemental Table 2). CD3 bsAbs were generated by cFAE of a high affinity human CD3 mAb with antibodies directed against different B cell antigens, that were either moderately (10,000-100,000 specific Abs bound per cell (sABC); CD22, CD24, CD70 and CD138) or highly (>100,000 sABC; CD20, CD37, CD79b and HLA-DR) expressed on all or a subset of malignant B cell lines. CD3 bsAbs targeting the different tumor antigens showed strong variation in cytotoxic capacity, as assessed in a 24-hour chrome release assay. CD3 bsAbs targeting the moderately expressed antigens CD22, CD24 and CD70 induced approximately 30%, 40% and 70% tumor cell kill, respectively. CD3 bsAbs targeting CD79b, CD37 and CD20,

FIGURE 2 **Studying the contribution of the CD20-specific Fab-arm to the potency of DuoBody-CD3xCD20.**
A: The indicated bsAbs were tested at a concentration of 1 µg/mL in triplicate in at least 3 different experiments using 2 different donors each, for their capacity to induce T cell-mediated cytotoxicity towards RI-1 (grey), RPMI-8226 (blue), Daudi (white) or OCI-Ly7 (black) target cells by adding them to a coculture of purified T cells and chrome-loaded target cells (E:T ratio 10:1). Target cell lysis was measured by chrome release after 24 h.
B: Binding of multiple CD3xCD20 (left), CD3xCD37 (**middle**) and CD3xCD70 (**right**) bsAbs to their TAA on Daudi cells was assayed by flow cytometry. Data shown are mean fluorescence intensities (MFI).
C: The capacity to induce T cell-mediated cytotoxicity was determined by the release of chromium from chromium-loaded Daudi cells after a 24 h coculture with purified T cells). Blue/purple and red/orange colors indicate bsAb with similar epitope regions. One representative donor out of 4 donors tested is shown.
D: EC_{50} values (µg/mL +/- SD; determined as described in M&M) for TAA binding and the induction of T cell-medicated cytotoxicity were calculated for the different bsAb and the average values are of at least 2 experiments with 2 donors per experiment are depicted (H). (ND= not determined)

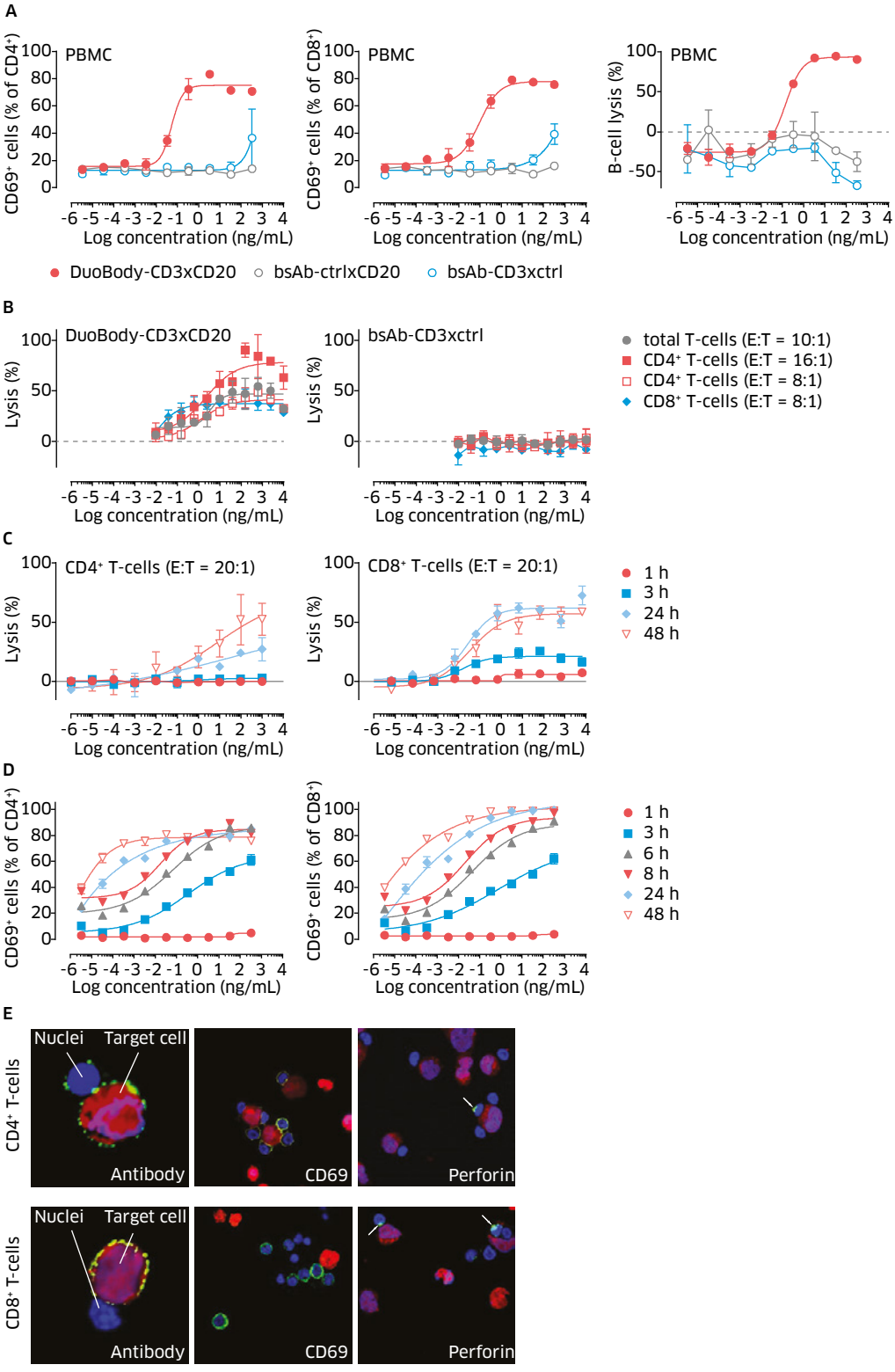
A
PBMC
CD69+ cells (% of CD4+)
CD69+ cells (% of CD8+)
B-cell lysis (%)
Log concentration (ng/mL)
DuoBody-CD3xCD20
bsAb-ctrlxCD20
bsAb-CD3xctrl
B
DuoBody-CD3xCD20
bsAb-CD3xctrl
Lysis (%)
total T-cells (E:T = 10:1)
CD4+ T-cells (E:T = 16:1)
CD4+ T-cells (E:T = 8:1)
CD8+ T-cells (E:T = 8:1)
C
CD4+ T-cells (E:T = 20:1)
CD8+ T-cells (E:T = 20:1)
1 h
3 h
24 h
48 h
D
6 h
8 h
E
CD4+ T-cells
CD8+ T-cells
Nuclei
Target cell
Antibody
CD69
Perforin

all of which showed high levels of target expression, demonstrated somewhat more efficient cytotoxicity: 50%, 80% and 80% tumor cell kill, respectively. Interestingly, none of the six different CD3 bsAbs targeting HLA-DR, which shows target expression levels comparable to or higher than CD20, were able to induce cytotoxicity, demonstrating that high levels of target expression do not guarantee efficacy of CD3 bsAbs (Figure 2A).

CD3 bsAbs specific for CD37 and CD70, that, together with DuoBody-CD3xCD30, showed the best results in our screen, were studied in more detail. For each target, including CD20, four different target-specific mAbs, selected for diversity in binding characteristics, were exchanged with a human CD3-specific IgG1 to generate the following CD3 bsAbs: DuoBody-CD3xCD20, CD3xCD20$_{2C6}$, CD3xCD20$_{Ritux}$, CD3xCD20$_{hu2H7}$, CD3xCD37$_{Ab1}$, CD3xCD37$_{Ab2}$, CD3xCD37$_{Ab3}$, CD3xCD37$_{Ab4}$, CD3xCD70$_{1F6}$, CD3xCD70$_{1F4}$, CD3xCD70$_{2H5}$ and CD3xCD70$_{10B4}$.

For each target, the four CD3 bsAbs could be divided into two groups based on their fine epitope specificity for CD20, CD37 or CD70, either based on binding cross block experiments (CD37 and CD70; supplemental Table 3) or on published epitope specificities (CD20 [22, 23]).

The relation between TAA binding characteristics (epitope, affinity) and the capacity of CD3 bsAbs to induce cytotoxicity was studied using Daudi cells as target cells, and purified healthy donor T cells as effector cells. Although target expression levels were not identical between the targets (CD37>CD20>CD70, supplemental Table 2), using the same cell line allowed comparison of the targets and antibodies without variability in target cells.

Target binding characteristics, such as EC_{50} and maximal binding, did not predict the capacity of CD3 bsAbs to induce T cell-mediated cytotoxicity (Figure 2B-D). For example, despite the differential binding pattern of CD3xCD20$_{2C6}$ compared to CD3xCD20$_{hu2H7}$ and CD3xCD20$_{Ritux}$ (Figure 2B), all three bsAbs displayed comparable cytotoxic activity in Daudi cells (Figure 2C). In contrast, DuoBody-CD3xCD20 induced considerably more potent cytotoxicity and also showed higher maximum levels of binding. The CD37-targeting CD3 bsAbs, CD3xCD37$_{Ab1}$, CD3xCD37$_{Ab3}$ and CD3xCD37$_{Ab4}$ showed quite different binding characteristics, but induced comparable cytotoxicity. CD3xCD37$_{Ab2}$ showed reduced binding, and reduced potency compared to the other CD3xCD37 bsAbs. For the CD70 bsAbs, the potency observed in Daudi cells was considerably lower than in RPMI-8226 cells that were used the first screen, despite higher expression of CD37 on Daudi cells (Supplemental Table 2). Nonetheless, also for CD70, the differences in potency of CD3 bsAbs could not be predicted based on the binding characteristics, as all were equally low in maximum binding levels.

Similarly, cytotoxic capacity of the CD3 bsAbs was unrelated to the epitope specificity of the CD20, CD37 or CD70-specific binding arms (Figure 2B-C). Even for the CD20-targeting CD3 bsAbs, where a clear difference in target binding characteristics was observed between the two epitope groups (Figure 2B left panel), this difference was not reflected in cytotoxic capacity (Figure 2C, left panel).

Taken together, target expression levels, or target binding characteristics and epitope specificity of the TAA-specific Fab-arm, could not foretell the potency of CD3 bsAb targeting CD20, CD37 or CD70 on malignant B cells. This shows that rationalized combination of a panel of antibodies does not guarantee the identification of a bsAb candidate molecule with the specific properties of DuoBody-CD3xCD20 as none of the other CD3 bsAbs could outcompete DuoBody-CD3xCD20 for its potent targeting of B cells in this *in vitro* cytotoxicity screening.

DuoBody-CD3xCD20 induced potent anti-tumor activity in humanized mouse models.

The anti-tumor activity of DuoBody-CD3xCD20 was assessed *in vivo* using CD20-positive lymphoma xenograft models in mice engrafted with human immune cells. In a co-engraftment model where NOD-SCID mice were injected SC with a 1:1 mixture of PBMC and Raji B cell lymphoma cells, followed by IV administration of antibody 2 hours later, DuoBody-CD3xCD20 induced a dose-dependent decrease in tumor outgrowth compared to PBS (Figure 3A). In the same model, we assessed the capacity of DuoBody-CD3xCD20 to exert anti-tumor activity in the presence of circulating rituximab (IgG1-RTX), which is known to compete with DuoBody-CD3xCD20 for CD20 binding (data not shown and [24]). To ensure that anti-tumor activity observed in this study could be attributed to DuoBody-CD3xCD20, the FEA mutations were introduced into IgG1-RTX to generate a variant (IgG1-RTX-FEA) that is not capable of inducing antibody-dependent cell-mediated cytotoxicity (ADCC) and complement-dependent cytotoxicity (CDC). At a dose of 0.05 mg/kg, DuoBody-CD3xCD20 induced potent anti-tumor activity, also in the presence of up to 10 mg/kg IgG1-RTX-FEA, indicating that DuoBody-CD3xCD20 treatment is not hampered by the presence of IgG1-RTX (Figure 3B).

The therapeutic potential of DuoBody-CD3xCD20 was assessed in humanized immune system (HIS) mice, using both an IV and a SC xenograft model [20]. Mouse hematopoietic stem cells were eradicated by sub lethal irradiation, followed by intrahepatic transplantation of human $CD34^+$ cord blood cells. After approximately 15 weeks, reconstitution of human lymphocyte populations in the mice was confirmed by flow cytometry (data not shown). For the orthotopic tumor graft settings, mice were injected IV with Daudi cells and Ab treatment was initiated 3 days later. Treatment with DuoBody-CD3xCD20, but not the control bsAb-CD3xctrl, resulted in a delay in tumor outgrowth (Figure 3C). After establishing efficacy in a model representing the leukemic phase of B cell malignancies, we mimicked the more solid manifestation of B cell lymphoma. HIS mice were implanted SC with Raji lymphoma cells and tumors were allowed to establish before Ab treatment was initiated. DuoBody-CD3xCD20 induced a profound inhibition of tumor growth at doses of 0.1 mg/kg and 1 mg/kg, whereas bsAb-CD3xctrl did not show anti-tumor activity (Figure 3D). Interestingly, bsAb-ctrlx-CD20 also induced some anti-tumor activity in this model. Besides the inhibitory effect on the SC tumor, this reconstituted HIS-model allows the study of depletion of normal human B cells in the circulation. Flow cytometry analysis at day 4, 9 and 16

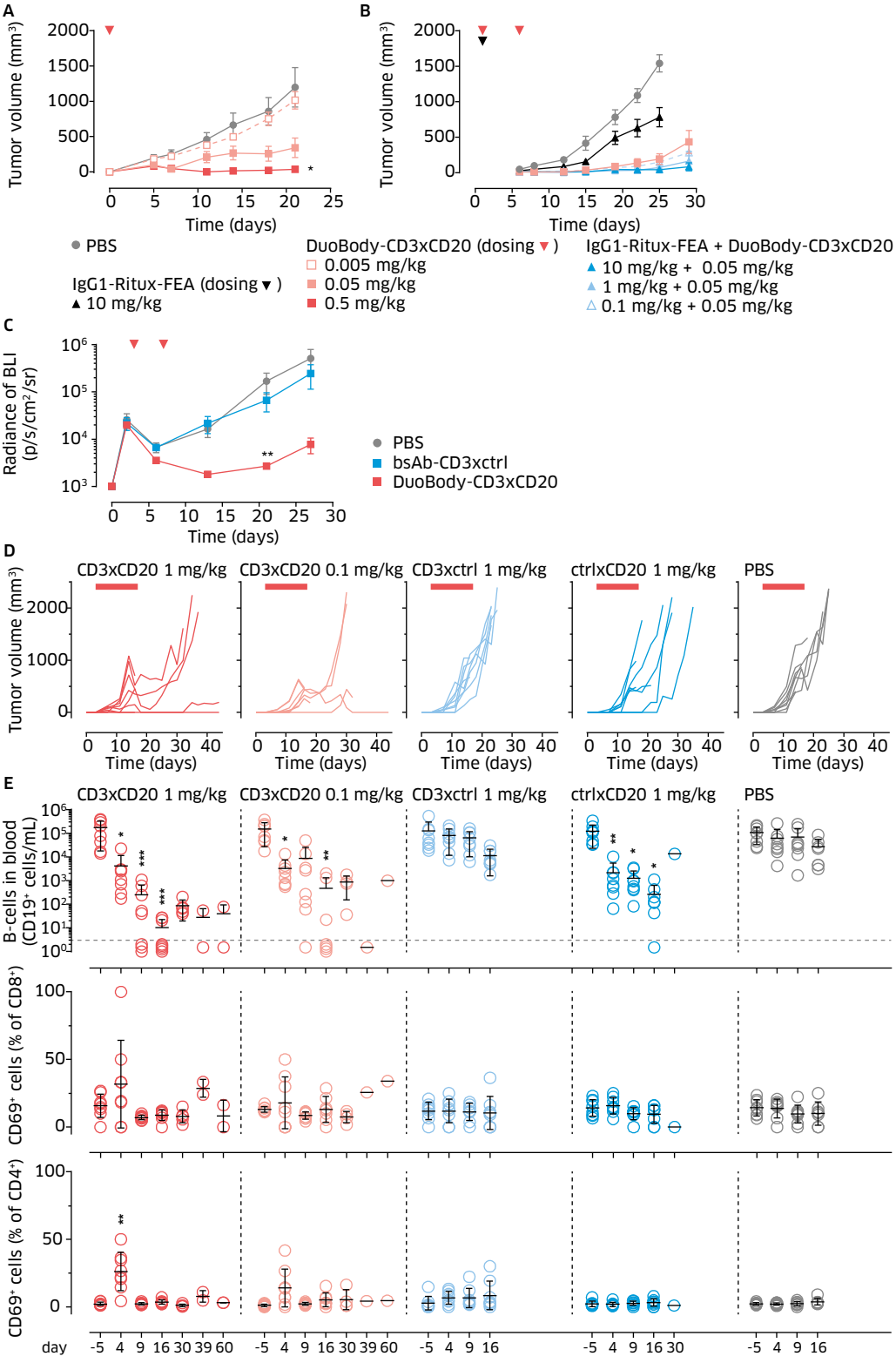
A
B
Tumor volume (mm³)
Time (days)
PBS
IgG1-Ritux-FEA (dosing ▼)
▲ 10 mg/kg
DuoBody-CD3xCD20 (dosing ▼)
0.005 mg/kg
0.05 mg/kg
0.5 mg/kg
IgG1-Ritux-FEA + DuoBody-CD3xCD20
▲ 10 mg/kg + 0.05 mg/kg
▲ 1 mg/kg + 0.05 mg/kg
△ 0.1 mg/kg + 0.05 mg/kg
C
Radiance of BLI (p/s/cm²/sr)
PBS
bsAb-CD3xctrl
DuoBody-CD3xCD20
D
CD3xCD20 1 mg/kg
CD3xCD20 0.1 mg/kg
CD3xctrl 1 mg/kg
ctrlxCD20 1 mg/kg
PBS
E
B-cells in blood (CD19⁺ cells/mL)
CD69⁺ cells (% of CD8⁺)
CD69⁺ cells (% of CD4⁺)
day
-5 4 9 16 30 39 60
-5 4 9 16
-5 4 9 16 30

revealed a decrease in circulating B cells after treatment with DuoBody-CD3xCD20 (0.1 and 1 mg/kg) and bsAb-ctrlxCD20 ($p<0.05$) compared to the PBS-treated mice (Figure 3E). In addition, in mice treated with DuoBody-CD3xCD20, a transient upregulation of the T cell activation marker CD69 was observed in peripheral blood $CD4^+$ and $CD8^+$ T cells at day 4 (Figure 3E). T cell activation was not observed in animals treated with bsAb-ctrlxCD20.

In summary, DuoBody-CD3xCD20 induced anti-tumor activity towards B-cell lymphoma cells at SC sites as well as in the blood circulation. This was paired with a transient T-cell activation, and was not hampered by the presence of circulating IgG1-RTX.

DuoBody-CD3xCD20 induced potent and long-lasting B cell depletion in cynomolgus monkeys after IV or SC administration

As part of the non-clinical safety studies, DuoBody-CD3xCD20 was administered to cynomolgus monkeys, the only standard toxicology species for which target binding characteristics and *in vitro* pharmacology of DuoBody-CD3xCD20 were comparable to humans. A single injection of DuoBody-CD3xCD20, administered IV or SC at doses of 0.01, 0.1, 1 or 10 mg/kg, induced a dose-dependent depletion of B cells from peripheral blood (Figure 4A, C) and lymph nodes (Figure 4B, D). B cell depletion was reversible at all dose levels, with time to recovery being inversely related to the treatment dose. B cell depletion was at least as efficient after SC compared to IV administration.

FIGURE 3 ***In vivo*** **evaluation of the efficacy of DuoBody-CD3xCD20.**
A-B: Tumors were induced in NOD-SCID mice by SC injection of a mixture of 5 x 10^6 human PBMC and 5 x 10^6 Raji-luc cells at day 0. Immediately after tumor inoculation, mice (5 per group) were treated with a single IV dose of DuoBody-CD3xCD20 (0.5, 0.05, 0.005 mg/kg) (**A)** or mice (10 per group) were given a single IV dose of IgG1-RTX-FEA (10, 1 or 0.1 mg/kg), followed by IV treatment with 0.05 mg/kg DuoBody-CD3xCD20 four hours later **(B)**. Data shown are mean tumor volumes per treatment group ± standard error of the mean (SEM). Differences were analyzed by Mann-Whitney two-tailed test versus PBS. Statistically significant differences are indicated as follows: * $p<0.05$ *** $p < 0.0005$ **** $p < 0.0001$.
C: Tumors were induced in BRGS-HIS mice by IV injection of Daudi-luc cells at day 0. Mice were treated IV with 1 mg/kg DuoBody-CD3xCD20 on day 3 and day 7. Tumor growth was evaluated by bioluminescence imaging (BLI) and depicted as average radiance of BLI ± SEM (7 mice per group);
D-E: Tumor growth of Raji-luc xenografts. Tumors were induced in BRGS-HIS mice by SC injection of Raji-luc cells at day 0. Mice were treated IV with 1 mg/kg or 0.1 mg/kg bispecific antibody or vehicle control on days 3, 7, 10, 14, and 17. Data are shown for each individual mouse, one graph per treatment group. Grey dotted lines indicate the tumor growth in PBS-treated mice. **E**. Individual (circles) and average (black line) absolute numbers of circulating human $CD19^+$ B cells determined by flow cytometry for the different treatment groups at multiple time points. Statistical significant differences compared to PBS treated mice at each time point were determined by Kruskall-Wallis analysis of variance (ANOVA) test with Dunn's multiple comparisons test. T cell activation was determined on indicated time points by flow cytometry. Individual (circles) and average (black line) percentages of $CD69^+$ cells in $CD4^+$ T cell population ($CD3^+CD19^-CD4^+$ events; **lower panel**) and $CD8^+$ T cell population ($CD3^+CD19^-CD8^+$ events; **mid panel**) is shown. Statistical differences compared to PBS-treated mice at the same time point were determined with Kruskall-Wallis ANOVA test followed by Dunn's multiple comparison test; * $p < 0.05$, ** $p < 0.01$ *** $p < 0.001$.

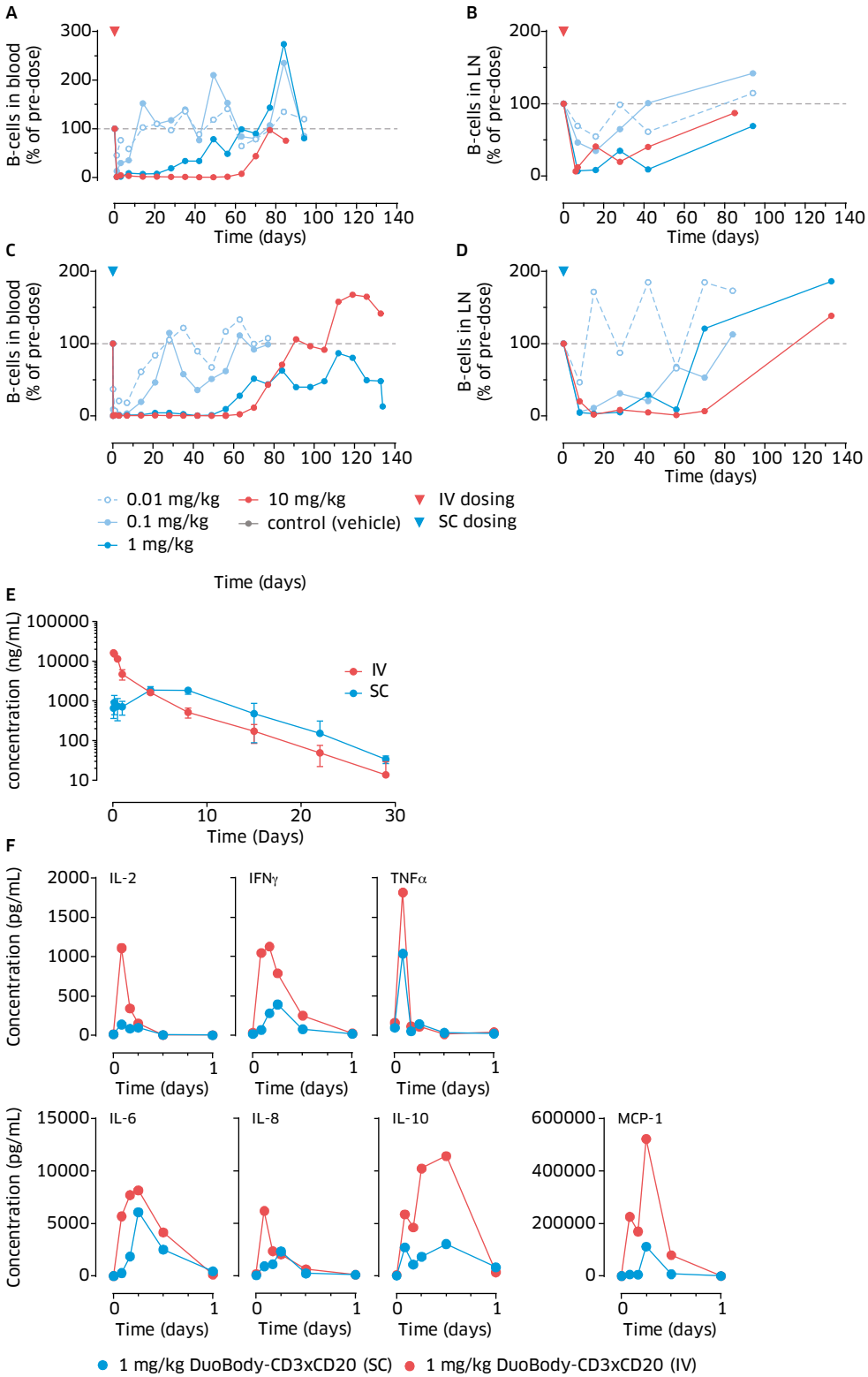
A
B-cells in blood (% of pre-dose)
Time (days)
B
B-cells in LN (% of pre-dose)
Time (days)
C
B-cells in blood (% of pre-dose)
Time (days)
D
B-cells in LN (% of pre-dose)
Time (days)
0.01 mg/kg
0.1 mg/kg
1 mg/kg
10 mg/kg
control (vehicle)
IV dosing
SC dosing
E
concentration (ng/mL)
IV
SC
Time (Days)
F
Concentration (pg/mL)
IL-2
IFNγ
TNFα
IL-6
IL-8
IL-10
MCP-1
Time (days)
1 mg/kg DuoBody-CD3xCD20 (SC)
1 mg/kg DuoBody-CD3xCD20 (IV)

Analysis of DuoBody-CD3xCD20 levels in plasma demonstrated different PK profiles for the IV and SC administration routes. Following IV infusion, the peak plasma concentration (C_{max}) was reached at the end of the 30-minute dosing period, to then decrease in a generally bi-phasic manner. After SC dosing, C_{max} was not reached until approximately three days after dosing and the plasma levels remained relatively steady up to seven days post dose (1 mg/kg, Figure 4E; 0.1 mg/kg Supplemental figure 3A). Thereafter, concentrations decreased in a mono-phasic manner up to the end of the four-week sampling period. At doses of 0.1 and 1 mg/kg DuoBody-CD3x-CD20, the peak plasma concentration was 7- to 17-fold higher after IV compared to SC dosing. Importantly, the exposure (area under the curve; AUC) of DuoBody-CD3xCD20 after SC or IV injection of a single dose of 0.1 and 1 mg/kg was comparable.
Injection of DuoBody-CD3xCD20 was associated with a rapid and transient increase in plasma cytokine levels. Interleukin (IL)-2, IL-6, IL-8, IL-10, interferon (IFN)γ, Tumor necrosis factor (TNF)α and monocyte chemoattractant protein (MCP)-1 reached peak levels within 2-12 hours after dosing (Figure 4F, supplemental figure 3B) and had resolved to baseline after 24 hours. For each of these cytokines, peak levels were considerably lower in animals that received SC dosing compared to animals that had been treated with the corresponding IV dose level. For IL-6, IL-8 and IFN-γ peak cytokine levels were reached somewhat later after SC compared to IV dosing, although for both administration routes plasma levels had returned to baseline at 12-24 hours.

In summary, DuoBody-CD3xCD20 induced profound and long-lasting depletion of B cells from peripheral blood and lymph nodes in cynomolgus monkeys that was comparable after IV and SC dosing. Peak plasma levels of DuoBody-CD3xCD20 were reduced after SC administration compared to IV administration and SC administration was associated with a considerable reduction in plasma cytokine levels.

DISCUSSION

DuoBody-CD3xCD20 is a novel CD20-specific CD3 bsAb that potently induces T-cell mediated cytotoxicity in the presence of CD20-positive B cells. To ensure that DuoBody-CD3xCD20 induced T cell activation only occurs in the presence of CD20-expressing cells, three point mutations (FEA) were introduced in the constant domain

FIGURE 4 Efficacy, PK and cytokine release evaluation of DuoBody-CD3xCD20 in cynomolgus monkeys.
A-D: Mean B cell counts ($CD19^+$ cells) are depicted per dose group (n=2) as a percentage of the B cell counts prior to dosing. Alterations in B cell counts in peripheral blood (**A, C**) and lymph nodes (**B, D**) are shown both after a single IV dose (0.01, 0.1, 1 or 10 mg/kg) and after a single SC dose (0.01, 0.1, 1, 10 mg/kg) of DuoBody-CD3xCD20.
E: Mean plasma concentration profiles for DuoBody-CD3xCD20 measured by SMCIA (Single Molecule Counting ImmunoAssay; 3 monkeys/group) after a single IV (red) or SC (blue) dose of 1 mg/kg DuoBody-CD3xCD20.
F: Mean cytokine levels measured in blood of monkeys using the Milliplex MAP NHP Cytokine Magnetic Bead Panel together with a BioPlex 200 reader (3 monkeys/ group) that received a single IV or a single SC dose of 1 mg/kg DuoBody-CD3xCD20.

of the antibody to abrogate FcγR and C1q binding.

DuoBody-CD3xCD20 induced potent anti-tumor activity *in vitro*. Intriguingly, while half-maximal binding (EC_{50} values) of the bsAb to CD20 on Daudi cells and CD3 on T cells occurred at Ab concentrations in the µg/mL range, T cell activation and cytotoxicity were already detected at more than 1,000-fold lower concentrations of the bsAb (EC_{50} values in low ng/mL range) (table 2, Figure 3). This reflects that already at sub-saturating concentrations of the bsAb, the effector T cell population could be induced to mediate potent efficacy. A similar observation was reported previously for epidermal growth factor receptor (EGFR) saturation with anti-EGFR antibody 2F8. Antibody-dependent cellular cytotoxicity (ADCC) was observed already when only 5% of the antigen was occupied by antibody, an observation that could directly be translated into an anti-tumor effect *in vivo* [25].

In an attempt to explain the contribution of the CD20-specific Fab-arm to the highly potent cytotoxicity of DuoBody-CD3xCD20, we generated a large panel of B cell-specific CD3 bsAbs by combining antibodies that target known B cell antigens with a CD3 bsAb platform using cFAE. An *in vitro* screen with this CD3 bsAb panel provided the opportunity to increase our understanding of antigen or antibody characteristics that affect CD3 bsAb efficacy. No correlation was observed between B cell antigen expression level (tested range: 300,000>10,000 molecules/cell) and CD3 bsAb efficacy. Absence of such a correlation has been described before [26], although we are the first to extend this observation across multiple TAA and multiple cell lines. Intriguingly, six different CD3 bsAbs targeting HLA-DR were unable to induce cytotoxicity, although HLA-DR showed the highest expression levels among the targets that were tested. The explanation for the lack of potency of CD3xHLA-DR bsAbs needs to be further explored, but may be related to disruption of the T cell/ B cell interaction, due to steric hindrance by the bsAb. Interestingly but unexpectedly, also no correlation was observed between target binding affinity of four different TAA-binding antibodies, targeting CD20, CD37, or CD70, and the CD3 bsAb cytotoxic potential. In addition, the antibody binding epitope was also found to be unrelated to the CD3 bsAb cytotoxic potential. These observations demonstrated that the excellent *in vitro* potency of the DuoBody-CD3xCD20 , could not have been predicted based on the characteristics of the 7D8 antibody clone.

Importantly, the *in vitro* potency of DuoBody-CD3xCD20 did translate to *in vivo* efficacy. It is complex to study the functionality of the human-specific DuoBody-CD3x-CD20 *in vivo* in mice, due to the absence of cross-reactivity of both arms with the murine antigens. Use of (double) transgenic mice is very complex. It was already shown by Ueda *et al.* [27] that for good translatability to the human system not only CD3ε, but also CD3γ and CD3δ should be humanized. Therefore, DuoBody-CD3xCD20 was not tested in such a model. The use of surrogate antibodies is an option to show that the concept works, but is not predictable for the investigated human-specific bsAbs. Therefore, we used HIS mice to test the anti-tumor efficacy of DuoBody-CD3xCD20 with the added benefit of a fully functional human T cell and human B cell repertoire

within the immune system of these mice [20]. B cell malignancies can manifest in the human body as a solid mass located anywhere in the body, and as liquid tumors located in the blood, both of which can be studied in the HIS model. In line with these two manifestations, HIS mice were treated with DuoBody-CD3xCD20 after an SC or IV challenge with CD20-positive tumors. DuoBody-CD3xCD20 induced activation of T cells and a reduction in $CD20^+$ cells both in the periphery (both tumor cells and normal B cells) as well as in the solid tumor mass. Because CD20-specific monoclonal antibodies are part of the standard of care for the treatment of B cell malignancies, many patients eligible for DuoBody-CD3xCD20 treatment will have received prior treatment with these antibodies. Resistance of B cell malignancies to CD20-targeting antibodies is not due to the loss of CD20 expression or CD20 mutation [28, 29], therefore a CD20-targeting antibody with a different mechanism of action compared to CD20-specific monoclonal antibodies may provide a powerful new strategy to treat CD20-expressing B cell malignancies. Importantly, it was shown in *in vivo* mouse models that DuoBody-CD3xCD20 is capable of inducing anti-tumor activity in the presence of circulating CD20 antibodies that compete for binding to CD20. Thus, patients that still have CD20 monoclonal antibodies in the circulation from a prior treatment line may still respond to treatment with DuoBody-CD3xCD20.

The promising *in vivo* results prompted investigation into the clinical validity of DuoBody-CD3xCD20 by assessing its safety in cynomolgus monkeys. which, due to the cross reactivity of both arms to the cynomolgus counterparts, also these studies allowed us to also study efficacy of the molecule in these animals, by measuring $CD20^+$ B cell depletion. DuoBody-CD3xD20 induced a potent, deep and reversible depletion of B cells from both peripheral blood and lymph nodes was observed in cynomolgus monkeys. These observations suggest superior efficacy of this bsAb over naked CD20 antibodies, which, as a monotherapy, have demonstrated excellent activity in leukemia (i.e. B cell depletion from blood), but reduced activity in lymphomas (i.e. B cell depletion from lymph nodes). Comparable efficacy of DuoBody-CD3xCD20 in cynomolgus monkeys was observed after SC and IV administration. Interestingly, data obtained at equivalent dosing showed that SC administration of DuoBody-CD3x-CD20 led to a lower C_{max} in combination with lower peak levels of plasma cytokines compared to IV administration. Since an important safety concern upon administration of CD3 bsAbs in the clinic is cytokine release syndrome, reducing cytokine levels by changing the route of CD3 bsAb administration might be an interesting scenario.

In conclusion, DuoBody-CD3xCD20 (GEN3013) is a novel CD3 bsAb specifically targeting CD20-positive B cell malignancies. Comparison with other CD3 bsAb targeting a variety of B cell antigens revealed that DuoBody-CD3xCD20 demonstrated superior potency *in vitro*. Moreover, DuoBody-CD3x-CD20 demonstrated anti-tumor activity in xenograft models *in vivo and* profound B cell depletion was observed in cynomolgus monkeys after intravenous or subcutaneous injections. These studies paved the way for clinical studies which are currently ongoing (NCT03625037).

REFERENCES

1 Topp, M.S., et al., *Phase II trial of the anti-CD19 bispecific T cell-engager blinatumomab shows hematologic and molecular remissions in patients with relapsed or refractory B-precursor acute lymphoblastic leukemia.* J Clin Oncol, 2014. **32**(36): p. 4134-40.

2 Viardot, A., et al., *Phase 2 study of the bispecific T-cell engager (BiTE) antibody blinatumomab in relapsed/refractory diffuse large B-cell lymphoma.* Blood, 2016. **127**(11): p. 1410-6.

3 Bluemel, C., et al., *Epitope distance to the target cell membrane and antigen size determine the potency of T cell-mediated lysis by BiTE antibodies specific for a large melanoma surface antigen.* Cancer Immunol Immunother, 2010. **59**(8): p. 1197-209.

4 Li, J., et al., *Membrane-Proximal Epitope Facilitates Efficient T Cell Synapse Formation by Anti-FcRH5/CD3 and Is a Requirement for Myeloma Cell Killing.* Cancer Cell, 2017. **31**(3): p. 383-395.

5 Moore, P.A., et al., *Application of dual affinity retargeting molecules to achieve optimal redirected T-cell killing of B-cell lymphoma.* Blood, 2011. **117**(17): p. 4542-51.

6 Fisher, T.S., et al., *A CD3-bispecific molecule targeting P-cadherin demonstrates T cell-mediated regression of established solid tumors in mice.* Cancer Immunol Immunother, 2018. **67**(2): p. 247-259.

7 Bacac, M., et al., *A Novel Carcinoembryonic Antigen T-Cell Bispecific Antibody (CEA TCB) for the Treatment of Solid Tumors.* Clin Cancer Res, 2016. **22**(13): p. 3286-97.

8 Labrijn, A.F., et al., *Efficient generation of stable bispecific IgG1 by controlled Fab-arm exchange.* Proc Natl Acad Sci U S A, 2013. **110**(13): p. 5145-50.

9 Labrijn, A.F., et al., *Controlled Fab-arm exchange for the generation of stable bispecific IgG1.* Nat Protoc, 2014. **9**(10): p. 2450-63.

10 Gramer, M.J., et al., *Production of stable bispecific IgG1 by controlled Fab-arm exchange: scalability from bench to large-scale manufacturing by application of standard approaches.* MAbs, 2013. **5**(6): p. 962-73.

11 Salmeron, A., et al., *A conformational epitope expressed upon association of CD3-epsilon with either CD3-delta or CD3-gamma is the main target for recognition by anti-CD3 monoclonal antibodies.* J Immunol, 1991. **147**(9): p. 3047-52.

12 Teeling, J.L., et al., *Characterization of new human CD20 monoclonal antibodies with potent cytolytic activity against non-Hodgkin lymphomas.* Blood, 2004. **104**(6): p. 1793-800.

13 Overdijk, M.B., et al., *Crosstalk between human IgG isotypes and murine effector cells.* J Immunol, 2012. **189**(7): p. 3430-8.

14 Vink, T., et al., *A simple, robust and highly efficient transient expression system for producing antibodies.* Methods, 2014. **65**(1): p. 5-10.

15 Engelberts, P.J., et al., *Type I CD20 Antibodies Recruit the B Cell Receptor for Complement-Dependent Lysis of Malignant B Cells.* J Immunol, 2016. **197**(12): p. 4829-4837.

16 Burton, D.R., et al., *Efficient neutralization of primary isolates of HIV-1 by a recombinant human monoclonal antibody.* Science, 1994. **266**(5187): p. 1024-7.

17 Da Roit, F., et al., *Ibrutinib interferes with the cell-mediated anti-tumor activities of therapeutic CD20 antibodies: implications for combination therapy.* Haematologica, 2015. **100**(1): p. 77-86.

18 Schneider, C.A., W.S. Rasband, and K.W. Eliceiri, *NIH Image to ImageJ: 25 years of image analysis.* Nat Methods, 2012. **9**(7): p. 671-5.

19 Brischwein, K., et al., *MT110: a novel bispecific single-chain antibody construct with high efficacy in eradicating established tumors.* Mol Immunol, 2006. **43**(8): p. 1129-43.

20 Legrand, N., et al., *Functional CD47/signal regulatory protein alpha (SIRP(alpha)) interaction is required for optimal human T- and natural killer- (NK) cell homeostasis in vivo.* Proc Natl Acad Sci U S A, 2011. **108**(32): p. 13224-9.

21 van Meerten, T., et al., *HuMab-7D8, a monoclonal antibody directed against the membrane-proximal small loop epitope of CD20 can effectively eliminate CD20 low expressing tumor cells that resist rituximab-mediated lysis.* Haematologica, 2010. **95**(12): p. 2063-71.

22 Teeling, J.L., et al., *The biological activity of human CD20 monoclonal antibodies is linked to unique epitopes on CD20.* J Immunol, 2006. **177**(1): p. 362-71.

23 Polyak, M.J. and J.P. Deans, *Alanine-170 and proline-172 are critical determinants for extracellular CD20 epitopes; heterogeneity in the fine specificity of CD20 monoclonal antibodies is defined by additional requirements imposed by both amino acid sequence and quaternary structure.* Blood, 2002. **99**(9): p. 3256-62.

24 Engelberts, P.J., et al., *A quantitative flow cytometric assay for determining binding characteristics of chimeric, humanized and human antibodies in whole blood: proof of principle with rituximab and ofatumumab.* J Immunol Methods, 2013. **388**(1-2): p. 8-17.

25 Bleeker, W.K., et al., *Dual mode of action of a human anti-epidermal growth factor receptor monoclonal antibody for cancer therapy.* J Immunol, 2004. **173**(7): p. 4699-707.

26 Seckinger, A., et al., *Target Expression, Generation, Preclinical Activity, and Pharmacokinetics of the BCMA-T Cell Bispecific Antibody EM801 for Multiple Myeloma Treatment*. Cancer Cell, 2017. **31**(3): p. 396-410.

27 Ueda, O., et al., *Entire CD3epsilon, delta, and gamma humanized mouse to evaluate human CD3-mediated therapeutics.* Sci Rep, 2017. **7**: p. 45839.

28 Gisselbrecht, C., et al., *Salvage regimens with autologous transplantation for relapsed large B-cell lymphoma in the rituximab era.* J Clin Oncol, 2010. **28**(27): p. 4184-90.

29 Johnson, N.A., et al., *CD20 mutations involving the rituximab epitope are rare in diffuse large B-cell lymphomas and are not a significant cause of R-CHOP failure.* Haematologica, 2009. **94**(3): p. 423-7.

30 Parren, P.W., et al., *Induction of T-cell proliferation by recombinant mouse and chimeric mouse/human anti-CD3 monoclonal antibodies.* Res Immunol, 1991. **142**(9): p. 749-63.

SUPPLEMENTARY DATA AND METHODS

Cell lines

The human cell lines Jurkat, NALM-6, HAL-01, 697, REH, RS4;11, NALM-16, MEC-2, JVM-3, JVM-2, Granta-519, JIYOYE, DB, DOHH-2, WSU-NHL and LP-1 were obtained from the Deutsche Sammlung von Mikroorganismen und Zellkulturen (DSMZ, GmbH, Braunschweig, Germany), and AU565, Mino, JVM-13, Daudi, Raji, Ramos, WIL2-S, ARH-77, SK-BR-3 and RPMI-8226 were obtained from the European collection of cell cultures (ECACC, Porton Down, UK). The Wien 133 cell line (Burkitt lymphoma cell line) was kindly provided by Dr. Geoff Hale (BioAnaLab Limited, Oxford, UK). IIA1.6-FcgR1 cells was kindly provided by Dr.Lisette Bevaart, UMC Utrecht, Dept. ImmunoTherapy, Utrecht, The Netherlands). SK-BR-3 cells overexpressing CD20 (SK-BR-3-CD20) were a kind gift from Thomas Valerius (University of Kiel). All cell lines were cultured according to supplier's instruction.

Quantitative analysis of antibody binding sites

Target expression, in terms of antibody binding sites (sABC), was analyzed using the QiFi kit (DAKO) according to manufacturer's instructions.

Cross-block of CD70 antibodies determined by biolayer interferometry

Antibody cross-block analysis (epitope binning) was performed using biolayer interferometry on an Octet HTX instrument (ForteBio). Antibodies (20 µg/mL in 10 mM sodium acetate buffer pH 6.0, ForteBio) were immobilized on Amine-Reactive 2nd Generation (AR2G) biosensors (ForteBio) according to the manufacturer's instructions. After a baseline measurement (100 s) in Sample Diluent (ForteBio), biosensors containing immobilized antibodies were loaded for 500 s with recombinant extracellular domain of CD70. Next, the association response of a second CD70 or CD37 antibody (10 µg/mL) was determined for 500 s. Measurements were performed at 30°C using a shaker speed of 1000 rpm. Data were analyzed using Data Analysis Software v9.0.0.12 (ForteBio). The Y-axis was aligned to the association step and Savitzky-Golay filtering was applied.

Cross-block of CD37 antibodies determined by flow cytometry

Binding competition between different CD37 antibodies was determined by flow cytometry. Raji cells (ATCC, CCL-86) were resuspended in Raji medium (RPMI 1640, 10% FBS, 100 U/mL penicillin, 100 µg/mL streptomycin, 10mM HEPES and 1mM pyruvate) at a concentration of 1x107 cells/mL. Next, 30 µL aliquots of the cell suspension were transferred into FACS tubes together with 30 µL aliquots (40 µg/mL final concentration) of unlabeled antibody solutions. The mixture was incubated at 37°C for 15 min while shaking gently. Next, A488-labeled antibody dilutions were prepared and after incubation, 10 µL of the labeled antibodies (4 µg/mL final antibody concentration) was transferred to the FACS tubes containing the unlabeled antibodies and cells. The mixture was incubated at 37°C for 15 min while shaking gently. After incubation, samples were quenched by adding 4 mL of ice cold PBS, centrifuged for 3 min at 4°C at 2000 rpm, aspirated twice and subsequent-

ly resuspended in 125 µL of PBS. Binding competition was analyzed by determining mean fluorescent intensities using a BD FACSCalibur (BD Biosciences). Fluorescence intensities were converted to Molecules of Equivalent Soluble Fluorochome (MESF) for quantitation.

AlamarBlue viability assay

Isolated T cells were suspended at a concentration of 5 x 10^6 cells/mL in assay medium). Antibodies were serially diluted in assay medium. Target cells were harvested by trypsinization (Trypsin-EDTA (0.5%), Gibco, cat. no. 15400-054) and suspended at a concentration of 0.25 x 10^6 cells/mL in assay medium.

SK-BR-3 or SK-BR-3-CD20 cells were used as target cells and were seeded (25,000 in 100 mL) in 96-wells flat bottom plates (Greiner cat. no. 655180) and left to adhere at 37°C, 5% CO_2 for 4 h. Supernatant was removed and 50 mL antibody (final concentrations of 1 x 10^{-7} – 1 mg/mL in 10-fold dilution steps) and 50 mL T-cell suspension were added and incubated at 37°C, 5% CO_2, for 48 h. Supernatant (including cells in suspension, i.e. T cells) was removed, and remaining cells were washed twice in PBS. 150 mL of a 10% alamarBlue solution (alamarBlue™ Cell Viability Reagent, ThermoFisher Scientific, cat.no. DAL1100; diluted in assay medium) was added to the adherent cells and incubated at 37°C, 5% CO_2 for 4 h. alamarBlue fluorescence was measured at 615nm (OD615) on an EnVision® plate reader (PerkinElmer). The percentage of viable cells was calculated using the following equation:

% viability = ($OD615_{sample}$/$OD615_{medium}$) x 100%

Proliferation assay

PBMCs were plated in 96-well flat-bottom plates (Greiner Bio-One, cat. no. 655180) (0.1 x 10^6 cells in 50 µL assay medium per well) and incubated with 50 µL/well of serially diluted antibody at a 2x concentration in assay medium (0.1 - 1,000 ng/mL final concentration; 10-fold dilution steps). After incubation at 37°C, 5% CO_2 for 72 h, 10 µL/well of 5-bromo-2′-deoxyuridine (BrdU) labeling solution, diluted 1:100 in assay medium was added to each well and plates were incubated at 37°C, 5% CO_2 for an additional 5 h. Cells were pelleted by centrifugation at 20 min at 800 x g, without brake. Supernatants were removed and plates were dried at 60°C for 1 h. Plates were stored at 4°C for a maximum of one week until the ELISA was performed.

T-cell proliferation was measured in a BrdU incorporation ELISA, according to the manufacturer's instructions. Cells were fixed and lysed with 200 µL/well of FixDenat at RT for 30 min; FixDenat was removed and 100 µL/well of peroxidase-labeled anti-BrdU-antibody solution (diluted 1:100) was added to each well and incubated at RT for 90 min. The antibody conjugate was removed and plates were washed three times in PBS, for ~ 5 min per wash. Washing solution was removed and binding of anti-BrdU antibody was quantified by addition of 100 µL/well of 2,2'-azino-bis(3-ethylbenzothiazoline-6-sulphonic acid (ABTS) buffer (Roche, cat. no. 11112597001) and incubation in the dark at RT for 30 min. Color development was stopped by addition of 100 µL/well 2% oxalic acid (Riedel de Haen, cat. no. 33506) and incubation at RT for 10 min. OD_{405} was measured on an EL808 Absorbance Microplate Reader (BioTek).

Cytokine release assay

Cytokines in supernatants from cytotoxicity assays were quantified using the ProInflammatory 9-Plex Tissue Culture Kit (Meso Scale Discovery, cat. no. K15007B-1), according to manufacturer's instructions. Briefly, 25 µL supernatant or calibrator sample was added to the multiplex plates, which were then sealed with adhesive plate seal and incubated with vigorous shaking (500 - 1,000 revolutions per min [RPM]) at RT for 1-2 h. 25 µL 1x detection antibody solution was added to each well, followed by another 1-2 h incubation period with vigorous shaking at RT. Plates were washed three times with PBS/0.05% Tween 20 (PBST: 10x PBS [Lonza, cat. no. 17-517]/0.5 % Tween 20 [Sigma Aldrich, cat. no. P1379]; diluted 1:10 in aqua dest. [B. Braun Medical B.V., cat. no. 3624331]) and 150 µL 2x Read Buffer T was added to each well. Chemiluminescence was measured on an ECL Imager (Mesoscale Technology: Sector S600 (ECL), cat. no. IC0AA-0). Cytokine concentrations were calculated using standard curves obtained from the calibrator samples.

C1q ELISA

Dilution series of antibodies (7 - 30,000 ng/mL; 4-fold dilution steps) were coated on ELISA plates (Greiner, cat. no. 665092). Plates were blocked with PBS/0.2% BSA for 1 h, followed by the addition of 3% normal human serum (CLB, cat. no. M0008), as a complement source. Plates were incubated at 37°C for 1h, and washed with PBST. Polyclonal rabbit anti-human C1q antibody solution (DAKO cat. no. A0136; diluted 1:4000 in PBST/0.1% gelatin [Sigma Aldrich, cat. no. 33223]) was added to the wells (50 mL/well) and plates were incubated at RT for 1h. Following incubation, plates were washed three times in PBST, and incubated with 50 µL/well horse radish peroxidase (HRP)-labeled swine anti-rabbit IgG-Fc antibody (DAKO, cat. no. P0399; diluted 1:10000 in PBST/0.1% gelatin) at RT for 1 h. Plates were washed with PBST and binding was detected using 100 µL/well ABTS (ABTS tablets [Roche, cat. no. 1111242001] in ABTS buffer [Roche, cat. no. 11112597001]). Color development was stopped after 30 min by adding 2% (v/v) oxalic acid (100 µL/well). OD405 nm was measured on an ELx808 Absorbance Reader (BioTek Instruments, Winooski, VT, USA).

Determination of FcgRI binding

IIA1.6-FcgRI cells were incubated with a dilution series of antibody (9.8 – 10,000 ng/mL; 4-fold dilution steps) at 4°C for 30 min. Cells were washed with FACS buffer and incubated with R-PE-labeled goat anti-human IgG (Jackson ImmunoResearch, cat. no. 109-116-097; 1:100 diluted in FACS buffer) at 4°C, for 30 min. Unbound antibodies were removed by washing with FACS buffer and cells were analyzed on a FACS Canto II.

Determination of *in vivo* plasma clearance

Plasma clearance of the antibodies was evaluated in 7-10-week-old CB17 SCID mice (CB17/Icr-*Prkdc*^{scid}/IcrIcoCrl; Charles River), three mice per group. Mice received a single intravenous (IV) dose of 100 mg (5 mg/kg) antibody in 200mL PBS. Blood samples were taken after 10 min; 3-6 h; and 1, 2, 7, 14, and 21 days and analyzed twice, on separate days, in a total human IgG ELISA. ELISA plates were coated with 2 µg/mL of mouse anti-human IgG-kappa antibody

(CLB, cat. no. M1268) in PBS, at 4°C, O/N. After blocking with PBS/0.2% BSA, plates were incubated with dilutions of blood samples at RT for 1 h. Plates were then washed with PBST and incubated with goat anti-human IgG-HRP (Jackson Immunoresearch, cat. no 109-036-097; 1:5,000 dilution in PBS/0.2% BSA) at RT for 1 h. Plates were washed and binding was detected using ABTS. Color development was stopped after 30 min, by adding 2% oxalic acid to the wells. OD_{405} nm was measured on an ELx808 Absorbance Reader. Plasma clearance rates (mL/day/kg) were calculated based on the area under the curve (AUC), according to the following equation: Plasma clearance = dose (µg/kg)/AUC (µg/mL/day).

SUPPLEMENTARY FIGURES

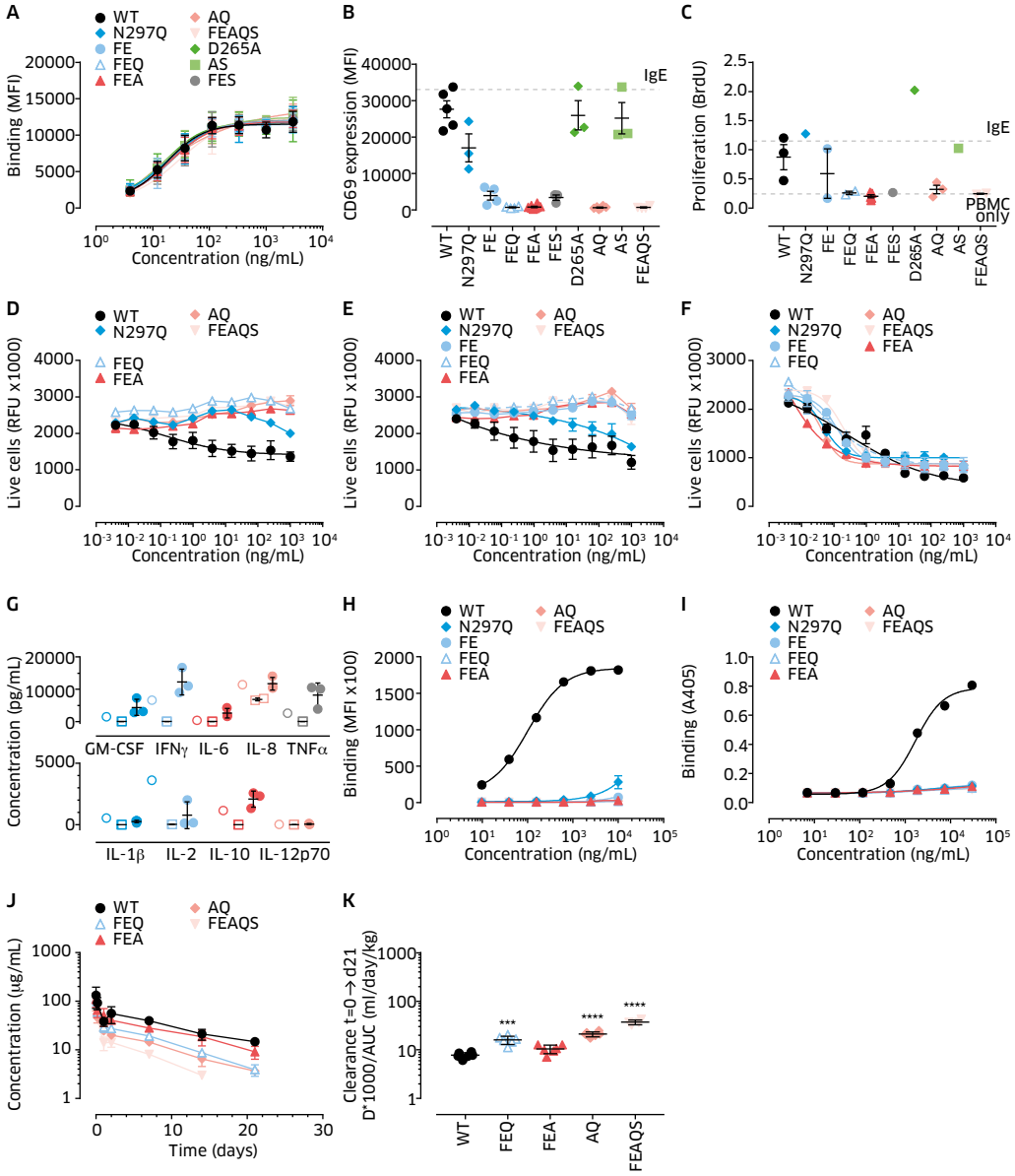

SUPPLEMENTARY FIGURE 1 Influence of inertness mutations on antibody characteristics.
A. The inertness mutations do not affect binding of the antibody to CD3⁺Jurkat cells, as determined by flow cytometry. Data shown is a representative figure of at least three replicates. Curves were fitted using non-linear regression curves: log(agonist) vs response – variable slope (four parameters). **B-C**. Applied inertness mutations vary in their ability to inhibit T cell activation as measured by flow cytometry-determined CD69 expression (B) or T-cell proliferation as measured by BrdU incorporation (**C**).
(**D-F**) TAA-expressing cell viability, measured by AlamarBlue conversion, after incubation with PBMCs and inert or non-inert IgG1-CD3* (**D**), DuoBody-CD3*xCtrl (**E**) DuoBody-CD3*xTAA (**F**), for three days. Data shown are mean RFU ± SEM. Dotted lines indicate 100% (upper line, medium alone) and 0% (bottom line, staurosporine) viability of TAA-expressing cells. Curves were fitted using non-linear regression curves: log(agonist) vs response – variable slope (four parameters).**G.** Release of the indicated cytokines was determined in supernatants of cytotoxicity experiments (three-day cocultures of PBMCs, TAAexpressing cells and the indicated antibodies by ELISA, using the ProInflammatory 9-plex Tissue Culture Kit. Data shown are mean cytokine levels ± SEM. **H.** Binding of inert and noninert antibodies to FcgRI expressed on IIa1.6 cells, analyzed by flow cytometry. Data shown is a representative figure of at least three replicates. **I**. C1q binding to plate-bound inert and non-inert IgG1-CD3* was measured by ELISA. Data shown is a representative figure of at least three replicates. Curves were fitted using non-linear regression curves: log (agonist) vs response – variable slope (four parameters). **J-K** *In vivo* clearance of inert and non-inert IgG1-CD3* were compared following a single IV dose in CB17 SCID mice (n = 3 mice per group). Blood samples were taken and analyzed twice (on separate days) by ELISA. Data represent mean concentration (µg/mL) ± SD of the two measurements for three mice. **J**. Clearance as measured by plasma concentration, **K**. Clearance as calculated from area under the curve (AUC).

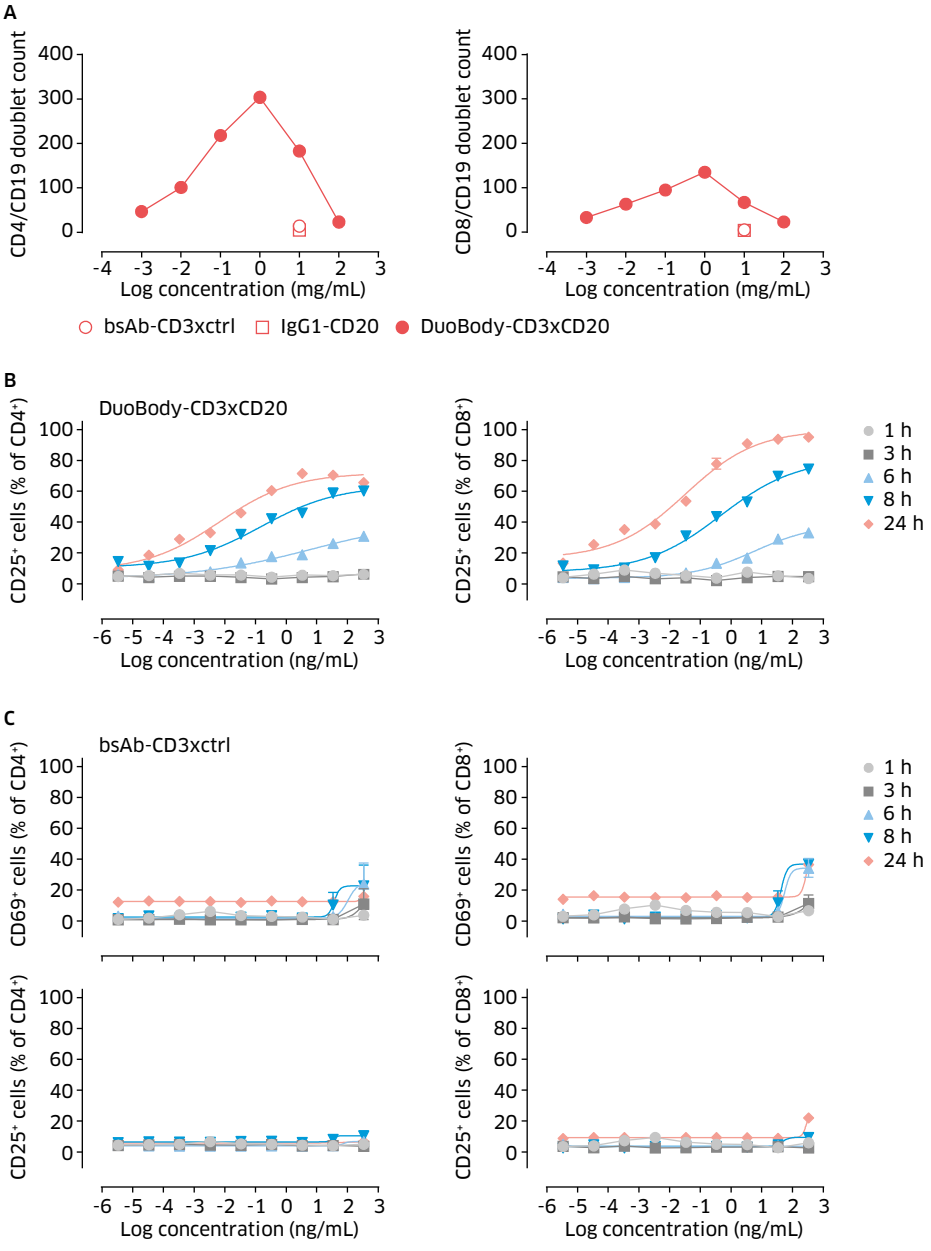
A
CD4/CD19 doublet count
CD8/CD19 doublet count
Log concentration (mg/mL)
bsAb-CD3xctrl
IgG1-CD20
DuoBody-CD3xCD20
B
DuoBody-CD3xCD20
CD25+ cells (% of CD4+)
CD25+ cells (% of CD8+)
Log concentration (ng/mL)
1 h
3 h
6 h
8 h
24 h
C
bsAb-CD3xctrl
CD69+ cells (% of CD4+)
CD69+ cells (% of CD8+)
CD25+ cells (% of CD4+)
CD25+ cells (% of CD8+)

SUPPLEMENTARY FIGURE 2 **DuoBody-CD3xCD20 mediated T cell / B cell cross linking.**
A: Whole blood was incubated with antibody for 48 h. The number of $CD19^+$ $CD4^+$ Double positive (**left**) and $CD19^+$ $CD8^+$ double positive) were determined by flow cytometry. Data shown are from one representative experiment out of 4 performed and are number of events per sample.
B-C: Freshly isolated T cells were incubated with DuoBody-CD3xCD20 (**B**) or bsAB-CD3xctlr (**C**) and CD20-expressing Daudi cells (E:T ratio 2:1).
B: Percentages of CD25-positive $CD4^+$ (**left**) and $CD8^+$ T cells (**right**) were determined at different time points, using the gating strategy indicated in M&M. Data for one representative donor out of four donors are shown. Graphs show the mean ± SEM of duplicate wells.
C: Percentages of CD69-positive $CD4^+$ (**upper left**) and $CD8^+$ T cells (**upper right**) and CD25-positive $CD4^+$ (**lower left**) and $CD8^+$ T cells (**lower right**) were determined at different time points, using the gating strategy indicated in M&M. Data for one representative donor out of four donors are shown. Graphs show the mean ± SEM of duplicate wells.

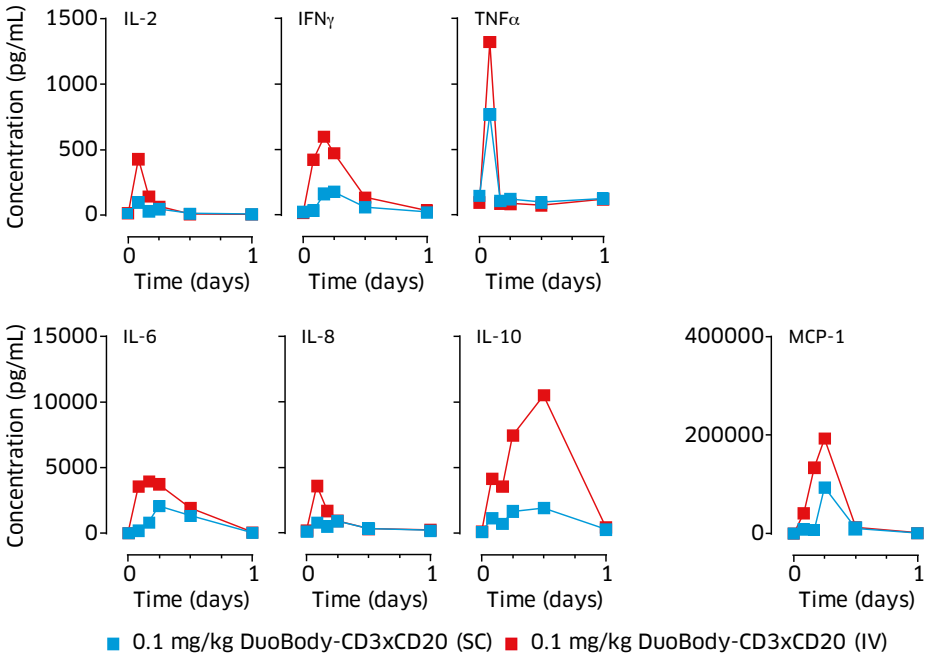

SUPPLEMENTARY FIGURE 3 **PK and cytokine release evaluation of DuoBody-CD3xCD20 in cynomolgus monkeys.**
A: Mean plasma concentration profiles for DuoBody-CD3xCD20 measured by SMCIA (Single Molecule Counting ImmunoAssay; 3 monkeys/group) after a single IV (**red**) or SC (**blue**) dose of 0.1 mg/kg DuoBody-CD3xCD20.
B: Mean cytokine levels measured in blood of monkeys using the Milliplex MAP NHP Cytokine Magnetic Bead Panel together with a BioPlex 200 reader (3 monkeys/ group) that received a single IV or a single SC dose of 0.1 mg/kg DuoBody-CD3xCD20.

SUPPLEMENTARY TABLES

SUPPLEMENTARY TABLE 1 Commercial antibodies used

Target	Label[1]	Clone	Supplier	Cat. No.	Used for
CD5	no	L17F12	BD Biosciences	345783	QiFi
CD10	no	Hi10a	BD Biosciences	555373	QiFi
CD19	no	4G7	BD Biosciences	347540	QiFi
CD20	no	mm7D8	Genmab	NA	QiFi
CD21	no	1048	BD Biosciences	552727	QiFi
CD22	no	HIB22	BD Biosciences	555423	QiFi
CD24	no	ML5	Miltenyi	130-098-502	QiFi
CD25	no	M-A251	BD Biosciences	555429	QiFi
CD37	no	IPO-24	Abcam	76521-100	QiFi
CD38	no	HIT2	BD Biosciences	555458	QiFi
CD40	no	5C3	BD Biosciences	555587	QiFi
CD46	no	M177	Monosan	MOU7066	QiFi
CD55	no	BRIC216	Chemicon	CBL511	QiFi
CD59	no	MEM43	serotec	MCA1054x2	QiFi
CD70	no	Ki-24	BD Biosciences	555833	QiFi
CD72	no	Bu40	Abcam	54000	QiFi
CD74	no	LN2	BD Biosciences	555612	QiFi
CD79a	no	ZL7-4	Serotec	MCA1298	QiFi
CD79b	no	SN8	southern	971001	QiFi
CD80	no	MEM-233	Abcam	ab8239	QiFi
CD95	no	DX2	BD Biosciences	555670	QiFi
CD138	no	nBT062	BD Biosciences	550804	QiFi
HLA-DR	no	L243	BD Biosciences	7360	QiFi
ROR1	no	2H6	Abcam	ab91187	QiFi
kappa	no	MH19-1	Sanquin	M1272	QiFi
lambda	no	1-155-2	BD Biosciences	345130	QiFi
IgG	no	MH16-1	Sanquin	M1268	QiFi
IgM	no	MH15-1	Sanquin	M1267	QiFi
CD45 /CD45	V500/BV711*	D058-1283	BD Biosciences	561489/ 740809	cynomolus flow cytometry panel
CD16	BV650	3G8	Biolegend	302042	cynomolus flow cytometry panel
CD4	FITC	L200	BD Biosciences	550628	cynomolus flow cytometry panel
CD19	APC	J3-119	Beckman Coulter	IM2470	cynomolus flow cytometry panel
CD8	APC-H7	SK1	BD Biosciences	560179	cynomolus flow cytometry panel

Target	Label[1]	Clone	Supplier	Cat. No.	Used for
CD3	EF450	OKT-3	eBioscience	48-0037-42	Human T cell activation/B cell depletion
CD4	APC-E780	OKT-4	eBioscience	47-0048-42	Human T cell activation/B cell depletion
CD8	AF700	RPA-T8	Biolegend	301028	Human T cell activation/B cell depletion
CD19	PerCP	SJ25C1	BD Biosciences	345790	Human T cell activation/B cell depletion
CD25	PE-Cy7	BC96	eBioscience	25-0259-42	Human T cell activation/B cell depletion
CD69	APC	AB2439	BD Biosciences	340560	Human T cell activation/B cell depletion
CD279/PD-1	BV605	EH12.2H7	Biolegend	329924	Human T cell activation/B cell depletion
mCD45	FITC	30-F11	Biolegend	103108	HIS mice flow cytometry panel
hCD45	PE/cy7	HI30	Biolegend	304016	HIS mice flow cytometry panel
hCD3	PE	UCHT1	BD Biosciences	555333	HIS mice flow cytometry panel
hCD19	APC	HIB19	Biolegend	302212	HIS mice flow cytometry panel
hCD4	BV605	OKT4	Biolegend	317438	HIS mice flow cytometry panel
hCD8	BV510	SK1	BD Biosciences	563919	HIS mice flow cytometry panel
Live/Dead	Indo-1	N/A	Invitrogen	L34962	HIS mice flow cytometry panel
CD69	FITC	FN50	BD Biosciences	555530	Confocal imaging
IgG	FITC	NA	southern	2042-02	Confocal imaging
perforin	A488	δG9	BD Biosciences	563764	Confocal imaging
Granzyme-B	FITC	GB11	BD Biosciences	560211	Confocal imaging

[1] FITC: fluorescein isothiocyanate; PE: phycoerythin; ECD: Electron coupled dye; BV: Brilliant violet; V: violet; Cy: cyanine dye; APC: allohphycocyanin ; A: AlexaFluor.

* During this study CD45 V500 was replaced temporarily with CD45 BV711 due to supplier issues. CD45 V500 was reinstated after supplier issues were resolved.

SUPPLEMENTARY TABLE 2 Cell surface expression of specific targets on a variety of cell lines.

		Pre B cell			B-ALL			CLL	
Antigen	Clone	NALM-6	HAL-01	697	REH	RS4;11	NALM-16	MEC-2	JVM-3
CD5	L17F12	0	0	0	0	0	9,5	0	0
CD10	Hi10a	98,2	61,1	27,2	63,4	0,7	70,3	0	0,5
CD19	4G7	61,3	48,5	58,5	34,6	38,9	31,1	15,5	10,6
CD20	7D8	11,1	32,9	97,8	19,8	0,7	81,8	167,7	186,8
CD21	1048	2,3	0,9	4,3	0	0,1	6,3	38,5	11,6
CD22	HIB22	6,7	7,7	14	5,5	5,7	21,3	33,8	14,6
CD24	ML5	ND	ND	ND	ND	ND	ND	ND	21,7
CD25	M-A251	3,3	0,2	1,2	0,5	0,3	1,2	2,4	2,4
CD37	IPO-24	8,6		23,2	4,9	11,4	13,9	33,7	119
CD38	HIT2	106,7	45,9	149,6	131,1	85,6	51,1	67,4	88,3
CD40	5C3	3,9	1,8	5	3,8	9,7	2,4	0	87,4
CD46	M177	30	31,9	64,1	50,1	38,1	56,4	44,7	47,5
CD55	BRIC216	26,2	6,1	0	2,8	18,2	8,1	22,7	19,3
CD59	MEM43	0,7	62,3	182,4	60,7	175,6	145,9	130,1	185
CD70	Ki-24	2,8	10,9	1,9	14,9	11,7	3,2	8,6	47,4
CD72	Bu40	27,2	11,9	22,2	15	23,6	36,5	12,6	3,9
CD74	LN2	10,4	12,7	16,3	9,1	4,8	3,5	17,7	16,8
CD79a	ZL7-4	4,6	1,2	18,7	0,9	1,4	2	4,7	2,8
CD79b	SN8	0,7	0	15,8	0	0	0	4,7	4,1
CD80	MEM-233	3,7	1,2	1,5	0,9	1,4	1,9	6,2	41,1
CD95	DX2	ND	4,1	2	1,9	6,7	4,7	0,7	1,3
CD138	nBT062	13,7	3,5	1,9	10,4	7,9	9,4	ND	11,4
ROR1	2H6	7,3	13,9	11,5	1,3	1,4	4	1,2	6,4
HLA-DR	L243	63,3	168	100,2	145,6	43,5	46,3	115	247
kappa	MH19-1	1,9	2,7	42,3	0,9	1	1	37,3	35,1
lambda	1-155-2	0	0	0	0	0	0	0,9	0,2
IgG	MH16-1	12	1,6	1,2	2,1	4,3	2,8	2,2	4,1
IgM	MH15-1	18,8	6,9	46,6	3,4	8,3	4,8	16,4	30,5

> 100,000 10,000-100,000 No binding detected ND Not determined

Target expression as assessed by antibody binding. The binding of various antibodies targeting antigens expressed on one or multiple B cell lines was determined using Qifi kit. Expression as measured in specific antibody bound (sABC) is noted in the table and associated with color (red, >100,000 sABC;; blue, between 10,000-100,000 sABC or no color, no binding detected).

		MCL					Burkitt				
Antigen	Clone	Mino	JVM-2	JVM-13	Jeko-1	Granta-519	Daudi	Raji	Ramos	Wien-133	JIYOYE
CD5	L17F12	20,5	0,1	0	3,6	0,9	0	0	0	0	0
CD10	Hi10a	0,3	0,2	0	9	0,5	28	20,8	44,9	20,8	4,5
CD19	4G7	97,2	6,3	4,4	22,9	8,5	1,1	62,2	0,5	33,9	21
CD20	7D8	359,3	122,1	169,1	250,2	347,6	132,6	173,7	222,1	102,4	37,8
CD21	1048	1,9	0,5	0,9	24	27,9	0	66,8	0,3	0,4	40
CD22	HIB22	5,9	14,8	6,8	1,6	11,1	79,8	39,5	28,2	13,2	14,3
CD24	ML5	ND	ND	7,1	ND	ND	5,2	ND	ND	ND	ND
CD25	M-A251	4,8	4,2	3,7	2,3	2,5	5,3	1,9	8	1	1,3
CD37	IPO-24	65,2	44,6	34,6	0	20,8	155	0	129,3	64,6	0
CD38	HIT2	209,7	127,3	98,3	42,8	91,1	199,2	170,2	262	91,8	66,5
CD40	5C3	43,9	0	0,8	28,3	28,9	2	69,7	1,7	16,1	123
CD46	M177	54	47	38	30,9	78	28,9	49,2	85	24,2	86,2
CD55	BRIC216	31,5	16,8	19,9	13,8	35,5	5,4	17,8	8,2	9,1	22,7
CD59	MEM43	150,2	185	140,2	27,6	201,1	3,6	55,7	50,7	9,6	159
CD70	Ki-24	48,1	ND	48,9	24,2	68,8	12,9	14,6	7,2	ND	35,2
CD72	Bu40	61,2	6,3	3,3	24,2	35,1	39,3	11,3	20,5	19	5
CD74	LN2	22,9	31,6	5,8	4,3	18,7	51,3	28,1	16,2	11,9	86,2
CD79a	ZL7-4	10,7	2,6	2,7	59	5,3	87,6	1,4	83,6	28	0,5
CD79b	SN8	16,2	1,1	3,8	68,9	5,4	111,3	1	101,2	29,2	0
CD80	MEM-233	5,2	9,3	5,7	4,1	4,8	5	29,5	1,7	0,7	56,8
CD95	DX2	2	0,8	0,2	1,7	22,2	2,3	45,6	0,1	0,5	67
CD138	nBT062	13,6	ND	13	15,2	9,6	4,3	4,3	3,9	ND	9,6
ROR1	2H6	19,9	2,2	1,1	13,8	4	1,3	4,1	0,8	11,2	2,1
HLA-DR	L243	481	267,5	98,5	233,1	312,1	205	126,8	141,3	34,1	240
kappa	MH19-1	1,3	0,6	0,3	179,1	1	161,1	6,4	0,5	40,8	13,5
lambda	1-155-2	28,2	5,1	9,2	0	12,8	3,3	0	87,8	2	0
IgG	MH16-1	5,8	3,3	3,3	6,2	3,3	3,7	5,9	2	5,4	0,5
IgM	MH15-1	46,7	7,6	15,4	163,4	10,8	149,6	8,2	171	52,4	0,5

		DLBCL							
Antigen	**Clone**	**SU-DHL-8**	**OCI-Ly19**	**OCI-Ly7**	**OCI-Ly18**	**SU-DHL-4**	**DB**	**RC-K8**	**RI-1**
CD5	L17F12	0	0	0,3	0	0	0,2	0,5	1,4
CD10	Hi10a	0,3	0,1	30,2	21,9	22,1	23	0,4	0
CD19	4G7	125	83,1	50,2	34	18	1,2	0,4	5,7
CD20	7D8	83,9	47,9	391,8	193,7	240,6	306,5	150,1	239
CD21	1048	1,7	0,8	20,7	3,5	7,6	1,9	0,5	ND
CD22	HIB22	4,9	4,1	49,7	14,4	25,6	7,2	2,2	15,8
CD24	ML5	ND	ND	48,5	ND	7	ND	ND	158
CD25	M-A251	0,2	0	13,5	2,4	1,6	5,1	6,3	ND
CD37	IPO-24	45,9	41,3	223,8	24,2	62,1	42	62	ND
CD38	HIT2	414,6	270,9	301,9	164,2	145,6	63,2	10,2	ND
CD40	5C3	52,3	41,6	53,3	8,2	19,3	88,3	0,4	87
CD46	M177	38,8	30,3	81,4	31,6	50,3	103	52	ND
CD55	BRIC216	24,5	18,8	17,2	13,9	18,1	37,3	31,6	8
CD59	MEM43	49,4	27,8	137,6	36,7	69,4	246,7	137,7	39,5
CD70	Ki-24	ND	ND	10	5,7	1	ND	2	5,6
CD72	Bu40	33,3	24,5	30,1	14,4	16,1	21,7	6,1	ND
CD74	LN2	14,2	12,6	87,2	38,3	22	3,3	17	ND
CD79a	ZL7-4	9,2	9,7	159,6	51,3	37,4	125,2	1,5	ND
CD79b	SN8	7,3	6,7	170,2	59,9	35,4	145,3	0,5	ND
CD80	MEM-233	26	24,5	5,5	8,4	8	15,7	9,6	10,4
CD95	DX2	0	8,3	6,7	0,2	6,5	3,9	0,9	ND
CD138	nBT062	8,9	ND	8,6	8,7	5,4	ND	10,5	10
ROR1	2H6	2,2	1,8	2,9	19,7	3,6	2,3	2,6	ND
HLA-DR	L243	223,7	248,6	311,5	220,6	162,6	1,6	143	ND
kappa	MH19-1	30,6	26	389,7	2,4	97,3	2,3	2,2	ND
lambda	1-155-2	2,2	1,2	2,3	0,5	0	128,4	0,5	ND
IgG	MH16-1	26	22,3	15,4	10,1	77,5	232,6	4,1	ND
IgM	MH15-1	1,7	0,7	341,6	133,7	7,6	6,4	0,8	ND

> 100,000 10,000-100,000 No binding detected ND Not determined

		FL		Plasmablast		MM	
Antigen	Clone	DOHH-2	WSU_NHL	WIL2-S	ARH-77	RPMI-8226	LP-1
CD5	L17F12	8,4	3,2	ND	0	0	0
CD10	Hi10a	35,4	34,3	0	0	5,8	1,5
CD19	4G7	20,5	40,9	2	0,2	0	0,1
CD20	7D8	249	339	ND	223	8	0,7
CD21	1048	4,3	1,3	ND	0,1	24,2	0,4
CD22	HIB22	33,9	84,2	ND	17,8	0	0
CD24	ML5	ND	ND	ND	ND	ND	7,314
CD25	M-A251	1,2	1,5	ND	1,2	0	0
CD37	IPO-24	81,4	42,7	ND	70,8	0	0
CD38	HIT2	147,3	47,8	85,7	25,6	159,3	134,4
CD40	5C3	1,2	48,4	50,7	0	7	1
CD46	M177	53,5	67	ND	63,8	102,1	47
CD55	BRIC216	33,1	8,7	ND	34,2	32,2	0
CD59	MEM43	79,4	145,5	ND	179,4	389,2	10,2
CD70	Ki-24	1,5	3,3	ND	29,3	3,9	1,9
CD72	Bu40	10,3	24,6	ND	12,3	1	1,1
CD74	LN2	21,9	36,1	ND	28,6	1,1	22,6
CD79a	ZL7-4	59,5	134,4	ND	6,3	1,1	0,5
CD79b	SN8	74	170,3	ND	5,3	0	0
CD80	MEM-233	3,6	9,1	ND	8,1	0,7	1,2
CD95	DX2	2	9,1	ND	0,3	19,5	38,9
CD138	nBT062	7,1	14,8	11,7	11,7	697	11
ROR1	2H6	1,6	1,4	ND	1,2	10,5	3,2
HLA-DR	L243	157	287	ND	214,9	0	141,8
kappa	MH19-1	0,7	2,1	ND	34,2	1,1	0,6
lambda	1-155-2	73,1	194,4	ND	0,4	0,9	25,5
IgG	MH16-1	23,9	116,9	ND	20,4	1,5	85,8
IgM	MH15-1	0,6	0,8	ND	0,7	3	1

SUPPLEMENTARY TABLE 3 **Cross-block of antibodies.**

	$CD70_{1F6}$	$CD70_{10B4}$	$CD70_{1F4}$	$CD70_{2H5}$
$CD70_{1F6}$	0	1	0	0
$CD70_{10B4}$	1	0	0	0
$CD70_{1F4}$	0	0	0	1
$CD70_{2H5}$	0	0	1	0

	$CD37_{Ab2}$	$CD37_{Ab4}$	$CD37_{Ab3}$	$CD37_{Ab1}$
$CD37_{Ab2}$	0	1	1	0
$CD37_{Ab4}$	1	0	0	1
$CD37_{Ab3}$	1	0	0	1
$CD37_{Ab1}$	0	1	1	0

0 No binding (Block) 1 Binding (no Block)

Antibody cross-block as determined by biolayer interferometry (CD70) and flow cytometry (CD37). Corrected association responses are shown. Cross-block of antibodies is indicated by the red color, non-blocking antibody combinations are indicated by the blue color.